Distribution Agreement

In presenting this thesis as a partial fulfillment of the requirements for a degree from Emory University, I hereby grant to Emory University and its agents the non-exclusive license to archive, make accessible, and display my thesis in whole or in part in all forms of media, now or hereafter now, including display on the World Wide Web. I understand that I may select some access restrictions as part of the online submission of this thesis. I retain all ownership rights to the copyright of the thesis. I also retain the right to use in future works (such as articles or books) all or part of this thesis.

Sihyun Jeon March 24, 2025

Effects of Renal N-methyl-D-aspartate Receptors in Regulating Renal Blood Flow and Hypertension.

by

Sihyun Jeon

Cesar A. Romero
Adviser

Department of Biology

Cesar A. Romero

Adviser

Leila Rieder

Committee Member

Jeanie Park

Committee Member

2025

Effects of Renal N-methyl-D-aspartate Receptors in Regulating Renal Blood Flow and Hypertension.

By

Sihyun Jeon

Cesar A. Romero
Adviser

An abstract of
a thesis submitted to the Faculty of Emory College of Arts and Sciences
of Emory University in partial fulfillment
of the requirements of the degree of
Bachelor of Science with Honors

Department of Biology

2025

Abstract

Effects of Renal N-methyl-D-aspartate Receptors in Regulating Renal Blood Flow and Hypertension

By Sihyun Jeon

N-methyl-D-aspartate receptors (NMDAr) are glutamate receptors that act as calcium channels. Previous research demonstrates that NMDAr in the kidney contribute to renal hemodynamics, potentially via interaction with epithelial sodium channel (ENaC) through a physiological mechanism not yet known. This thesis investigates how the NMDAr profile in the kidney contributes to blood pressure phenotype, specifically through scrutinization of the NMDAr subtypes. We evaluated change in blood pressure in response to NMDAr inhibition in Liddle Syndrome (LS)—a genetic disorder with overactivation of ENaC—mice in under normal (0.4% NaCl) and high salt (HS, 4% NaCl) diet. We repeated the experiment with GluN2C—a specific NMDA receptor subunit—antagonist to evaluate subtypical implications. GluN2C expression was confirmed and quantified via RNAscope and immunofluorescence. We also traced renal blood flow (RBF) in response to NMDAr inhibitor injection to gain mechanistic insight on the results. LS mice on normal salt diet exhibited acute increase in blood pressure upon NMDAr inhibition (SBP 130.2 ±14 vs. 104.3±17 mmHg, β=1.33 vs 1.116, $p<0.01$), followed by subacute normalization. Male LS mice on HS diet displayed elevated BP in response to increase in dietary sodium intake, and they exhibited acute decrease in BP subsequent to infusion of NMDAr inhibitor (SBP 96.1±2.5 vs. 126.8±25, $p<0.001$). Female cohort did not develop salt-sensitive hypertension, indicating sex difference. GluN2C-specific inhibition under normal salt diet displays similar phenomenon as non-selective inhibition (155.2±6 vs 108±1.6 mmHg, $p=0.008$). RNAscope results confirm GluN2C expression among LS and WT animals with no significant difference among cohorts. Immunofluorescence results demonstrate that WT males display significantly less GluN2C level compared to LS cohort, (437.3±172.3 vs. 1506±360, $p<0.01$), while the females displayed apparent reciprocal results (WT 1316±371.8 vs LS 590±172.5 $p=0.05$). Spectral analysis of RBF tracing indicates decrease in connecting tubule glomerular feedback (CNTGF) upon NMDAr inhibitor injection (0.22±0.1 vs 0.08±0.04, $p=0.03$). Results demonstrate that change in blood pressure in response to NMDAr inhibition on LS mice depends on dietary sodium intake and sex. There is significant difference in translation of GluN2C across genotype and sex, but not in transcription. NMDAr inhibition decreases CNTGF but does not alter total RBF.

Effects of Renal N-methyl-D-aspartate Receptors in Regulating Renal Blood Flow and Hypertension.

By

Sihyun Jeon

Cesar A. Romero
Adviser

A thesis submitted to the Faculty of Emory College of Arts and Sciences
of Emory University in partial fulfillment
of the requirements of the degree of
Bachelor of Science with Honors

Department of Biology

2025

Acknowledgements

Firstly, I express my sincerest gratitude to my thesis advisor and mentor Dr. Cesar Romero, who always provided invaluable support and guidance in my research for the past three years. I also genuinely thank my thesis committee members Dr. Leila Rieder and Dr. Jeanie Park for their time and effort in providing me with feedback and support, ultimately possibilitating this thesis. I thank my predecessor Heeju Jasmine Lim for connecting me with such an amazing research opportunity, and our lab coordinator Veronica Posse for providing valuable support in data collection and in editing of this thesis. I thank Emory School of Medicine Department of Pharmacology and Dr. Stephenson Traynelis for provision of essential drug used in part of this thesis. I acknowledge Emory Summer Undergraduate Program in Renal Research (SUPERR) (Grant ID: DK101390) for their financial assistance over summer of 2024. Lastly, I express substantial appreciation for my friend Joy H. Lee in helping me generate a number of figures and diagrams, as well as my family members and close friends who gave me constant love and support through it all.

Table of Content

I. Introduction

Hypertension (HTN), otherwise known as high blood pressure, is a medical condition in which the hydrodynamic pressure of the blood against the walls of arteries becomes chronically elevated within an individual, damaging the arteries and thereby significantly increasing risks of critical medical emergencies such as myocardial infarction, congestive heart failure, cerebrovascular accident, and end-stage renal disease requiring hemodialysis.[1] The kidney is known to play a crucial role in maintenance of homeostasis in context of blood pressure, specifically by controlling water-electrolyte balance within an organism—regulation of sodium (Na^+) and potassium (K^+) retention and/or blood plasma volume, which in turn directly impacts change in blood pressure.[2] Consequently, the kidney is one of the key therapeutic target in treating HTN, thereby effectively lowering mortality from the medical emergencies listed above.[1]

Though the medical etiologies of HTN can vary significantly, there is known positive correlation between increase in dietary sodium intake and blood pressure—the increase in blood pressure after a high sodium chloride load is known as salt-sensitive HTN.[3] Though specific physiological mechanisms behind salt-sensitive HTN are not very well understood, it seems that the blood pressure increase resets sodium excretion to keep the Na^+ level balanced, but to a new set point of blood pressure.[4] As a result, understanding the physiological and molecular mechanisms of the kidney with respect to prevalent alkali metal ions are critical in predicting development of HTN.

a. Structure of the Nephron

The nephron is the fundamental functional unit of the kidney that carries out numerous physiological processes including filtering blood, regulating water and electrolyte balance, and eliminating waste products via urine.[5] Each kidney in a healthy individual contains approximately 1 million nephrons. Each nephron is organized into the renal corpuscle, proximal convoluted tubule, loop of Henle, distal convoluted tubule, and the collecting duct (Figure 1).

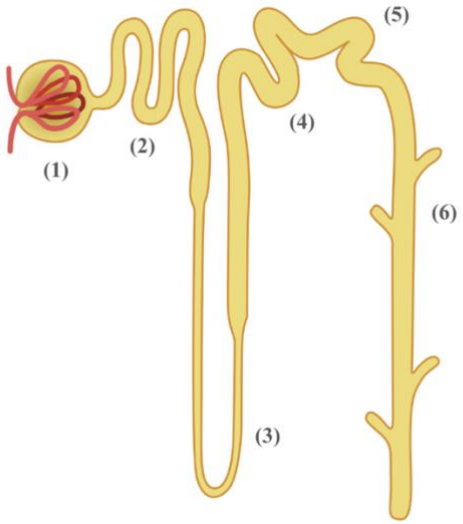

Figure 1: Structure of the Nephron. (1) Renal corpuscle, (2) proximal convoluted tubule, (3) loop of Henle, (4) distal convoluted tubule, (5) connecting tubule, (6) cortical collecting duct (Figure generated by Joy H. Lee).

Blood enters the nephron at a high pressure through the afferent arteriole, which turns into the blood filtration unit named the glomerulus at the renal corpuscle.[6] The pressure gradient promotes filtration of small solute molecules out of the capillaries and into the Bowman's capsule, where the tubular segment of the nephron begins. The filtrate then flows through the proximal convoluted tubule, the loop of Henle, and the distal convoluted tubule accordingly, where filtrate concentration adjustment occurs based on the physiological demand at a given timepoint. The filtrate ultimately enters the collecting duct, where final water reabsorption occurs before it is transported to the renal pelvis for excretion as urine.[7]

Approximately 60% of the filtered water and sodium filtered is bulk reabsorbed in the first segments of the nephron, while the 20% is reabsorbed in the loop of Henle paired with the concentration mechanism of the kidney, thus in the distal nephron segments is where the fine tuning of water and sodium reabsorption occurs.[8] In the connecting and collecting ducts, a plethora of signaling can regulate specific ion channels in accordance with homeostatic necessities—for example, the cells in connecting tubule utilize the epithelial sodium channel (ENaC) for reabsorption of around 5% of the filtered sodium, especially when the hormones angiotensin II and Aldosterone are elevated.[9] Apical membrane of the tubular cells comprising the nephron are populated with various receptors and ion channels, which dictate physiological functionality of the nephron accordingly. As a result, insight on interaction mechanisms between the channels is vital to understanding the function of the kidney, as well as its ultimate contribution to blood pressure phenotype.

b. Renal Blood Flow

Renal blood flow (RBF) refers to the blood volume delivered to the kidney per unit time.[10] RBF constitutes around 20% of cardiac output, which substantially exceeds the metabolic demand of the renal tissue; this corresponds to filtration of the blood and excretion of the metabolic waste, which is the main function of the kidney.[10] Blood enters the kidney via renal arteries, which branches into the interlobar artery that runs parallel to the corticomedullary junction. From there, the artery gives rise to numerous afferent arterioles that enter the nephron as glomerular capillaries (Figure 2).

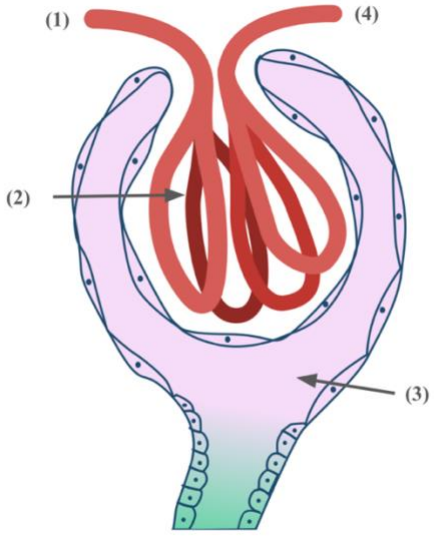

Figure 2: Structure of Glomerulus. (1) Afferent arteriole, (2) glomerular capillaries, (3) Bowman's capsule, (4) efferent arteriole. (Figure generated by Joy H. Lee)

RBF directly impacts the glomerular filtration rate (GFR), which is directly proportional to an individual's kidney functionality; consequently, regulation of RBF is critical in maintaining GFR at a steady level.[11] Renal autoregulation includes at least two feedback mechanisms, integrating tubular flow with RBF[7]; tubuloglomerular feedback induces vasoconstriction of the afferent arteriole in the presence of high flow in the macula densa and/or at the loop of Henle. The mechanism decreases RBF and correspondingly GFR, to avoid an excessive loss of fluid. On the other hand, if salt and water excretion is necessary, another feedback mechanism can induce an afferent arteriole vasodilation and correspondingly increase GFR instead.[12] This mechanism, namely connecting tubule-glomerular feedback, occurs at the connecting tubule and is known to be initiated by ENaC when high sodium or flow is detected in the connecting tubule.[13] Spectral analysis of RBF, study oscillatory patterns in physiological data and refers to the decomposition of a signal (e.g., renal blood flow oscillations) into its constituent frequencies. It typically involves techniques such as Fourier Transform or Wavelet Transform to examine how different frequency components contribute to the overall signal.[14] In the context of renal blood flow, spectral analysis helps identify characteristic frequency bands related to physiological processes such as myogenic, tubuloglomerular feedback, and neurogenic mechanisms.[15,16] Power analysis quantifies the magnitude (or energy) of oscillations at different frequencies, often derived from spectral analysis. It involves computing the power spectral density, which represents how the power of the signal is distributed across various frequency components. Higher power in specific frequency bands can indicate the dominance of certain regulatory mechanisms in renal blood flow dynamics.

c. N-methyl-D-aspartate Receptors

N-methyl-D-aspartate receptors, more commonly known as NMDA receptors, are glutamate receptors that act as calcium (Ca^{2+}) channels.[17] These channels are hetero-tetramers constituted by two mandatory subunits GluN1 combined with two variable subunits—GluN2A-D or GluN3A-B.[18] The distinguishable subtypes correspond to localization and channel dynamics. (Figure 3)

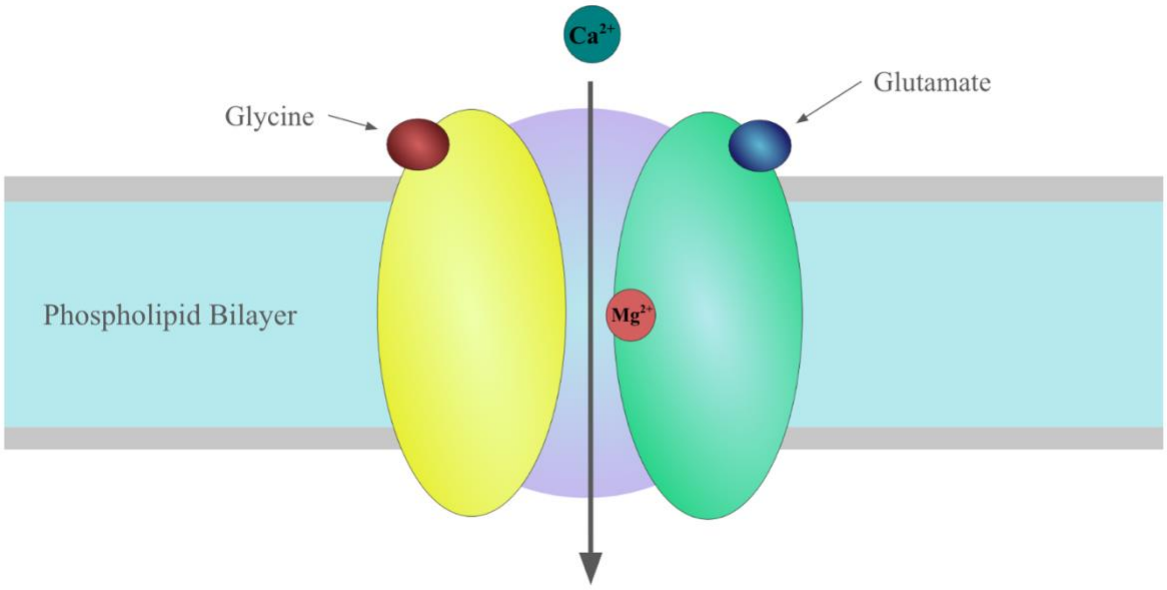

Figure 3: Structure of NMDA receptor. NMDA receptors are heterotetramers composed of 4 subunits. Functional receptor contains 2 GluN1 subunits and a combination of either GluN2A – GluN2D or GluN3A – GluN3B. Each receptor has a glutamate and glycine binding site, which either activates or inhibits the channel. (Figure generated by Joy H. Lee)

NMDA receptors most typically studied in the central nervous system.[17] However, NMDA receptors are also known to be ubiquitously present in most tissues.[19,20] With regards to the receptors in the kidney, previous research has shown that the receptor contributes to renal hemodynamics regulation.[19] Renal blood flow regulation in the kidney is critical in numerous renal processes, including sodium excretion and blood pressure regulation.[21] Previous research shows that decrease in renal blood flow induces increased blood pressure due to multiple mechanisms, likely secondary to difficulty in sodium excretion and activation of compensatory mechanisms such as the renin-angiotensin system.[22] The consequence of this blood pressure increase is known as pressure-natriuresis, where the kidney resets sodium excretion to keep its Na^+ level balanced, but to a new, elevated set point of blood pressure.

Previous research in our laboratory demonstrates that NMDA receptors interact with the epithelial sodium channels (ENaC), where activating NMDA receptors corresponds to an increase in activity of ENaC.[23] We also showed that this interaction induces an activation of connecting tubule glomerular feedback (CNTGF), a renal vasodilator mechanism that can potentially alleviate the increase in blood pressure by increasing sodium and water tubular load and excretion.[13] Nonetheless, the main effect of NMDA receptor activation or inhibition on blood pressure is not yet known. Thus, renal NMDA receptors' effect on blood pressure may be paradoxical—NMDA receptor inhibition can decrease vasodilation which then leads to increased blood pressure, while its inhibition of ENaC can correspond to decrease in sodium reabsorption and correspondingly cause a decrease in blood pressure (Figure 4).[13] Primary

emphasis of this research, in continuation of prior research conducted, involves uncovering how the NMDA receptor profile in the kidney contributes to blood pressure phenotype, specifically through investigation of the NMDA receptor subunits.

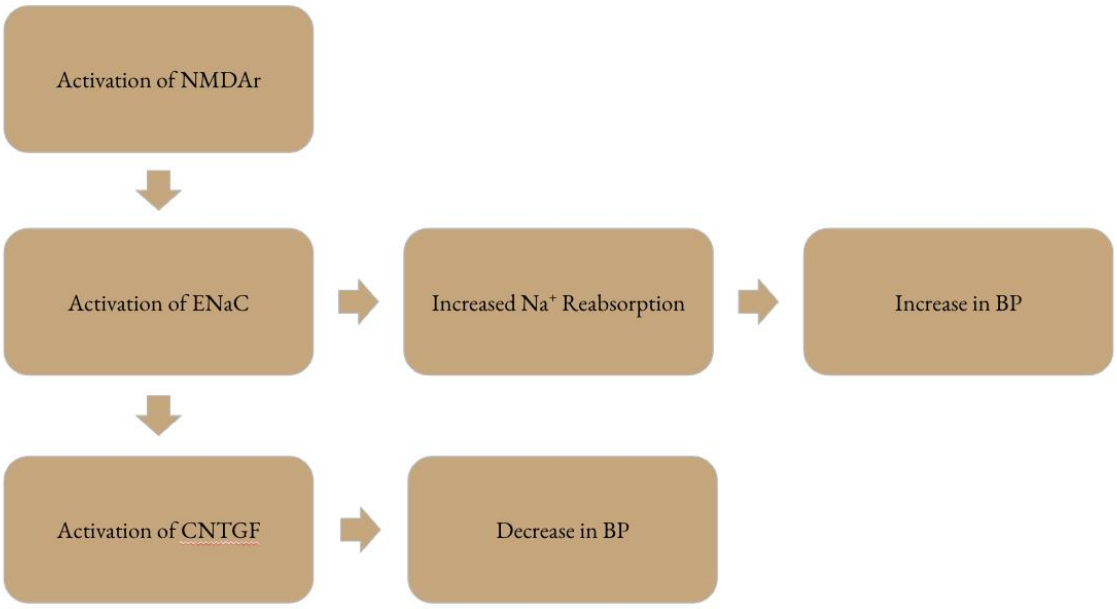

Figure 4: Paradoxical implications of NMDA receptor's contribution to blood pressure: NMDA receptor activation leads to increase in ENaC activity, which can potentially increase blood pressure via increase in Na^+ reabsorption. On the contrary, increase in ENaC activity leads to activation of CNTGF, which can potentially decrease blood pressure through increased GFR.

d. Liddle Syndrome

Liddle Syndrome (LS) is a rare genetic disorder characterized by overactivation of the ENaC and is known to be associated with medical conditions such as early onset HTN and hypokalemic metabolic alkalosis.[24] Though there are multiple known mutagenetic etiologies behind LS, the most common form arises from a point mutation in the genes that encode for the α, β, and γ subunits of ENaC—SCNN1A, SCNN1B, and SCNN1G respectively—which eliminates the channel's ubiquitination site.[24] Consequently, the channel cannot be degraded via cytosolic proteasome mechanism and thus proper internalization of the apical membrane is halted (Figure 5). Such a phenotype results in excessive renal sodium reabsorption in distal nephron, which then corresponds to arterial HTN due to expansion of intravascular volume and hypokalemia secondary to increased potassium secretion.[25] Evidently, these medical conditions are often heavily dependent on the individual's dietary sodium intake, and it is a form of salt-sensitive hypertension.[25] In mice with ENaC gain-of-function mutation as such, the hypertensive phenotype only appears when high salt diet is administered.[26,27]

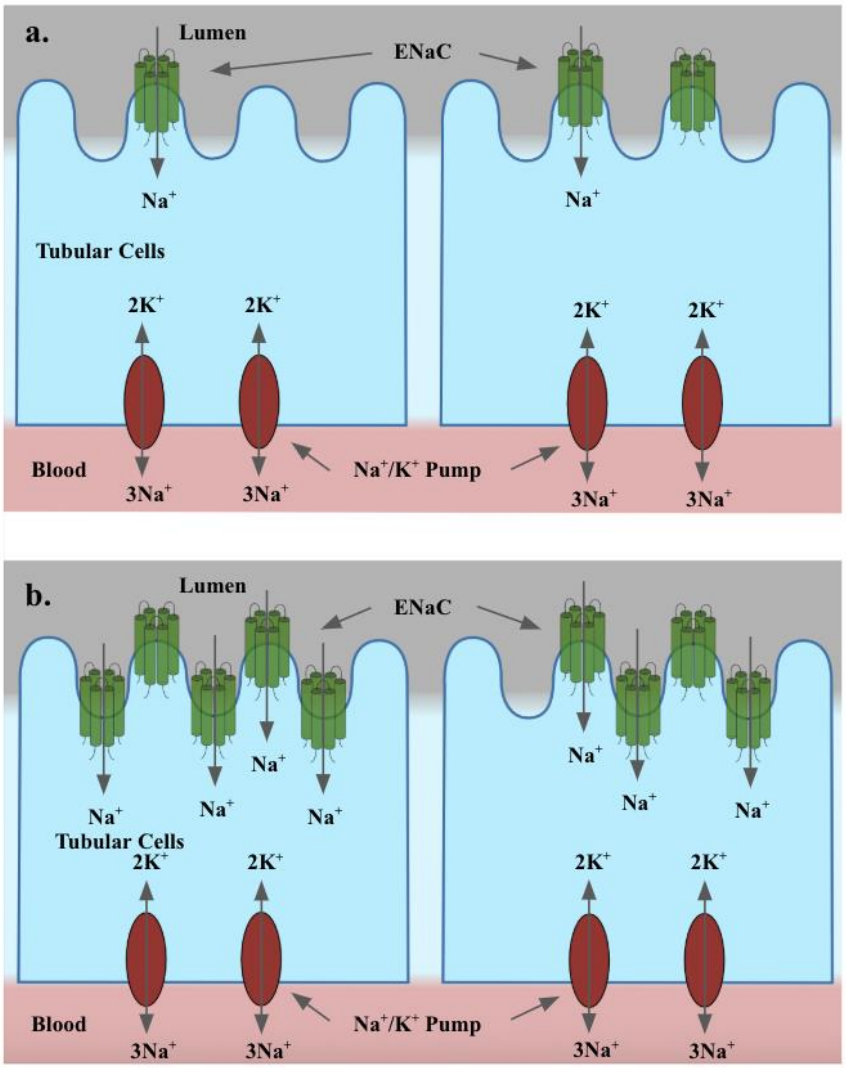

Figure 5: ENaC are hyperactive in LS. (a.) Wild type tubule versus (b.) Liddle Syndrome; deletion of critical ubiquitination site corresponds to inhibition of proper membrane internalization. Consequently, a large quantity of ENaC remain in the apical membrane of the tubular cells. (Figure generated by Joy H. Lee)

e. Hypothesis & Research Objective

Given the phenotypical characteristics as described above, the relationship between ENaC and renal NMDA receptor activity would be accentuated in LS mice; correspondingly, we primarily utilized the LS strain in all experimental methodology delineated below. We hypothesize that inhibition of NMDA receptors in LS mice will have a dual effect; we expect acute increase in blood pressure due to the inhibition of CNTGF and the consequent vasoconstrictions, followed by subacute decrease in the blood pressure due to the inhibitory effect on ENaC and reduction of sodium reabsorption. This thesis consists of three research objectives accordingly:

1. Investigate the effect of NMDAr inhibition on blood pressure phenotype.

2. Analyze implications on specific NMDAr subtypes expression.

3. Evaluate acute effect of NMDAr inhibition on RBF and CNTGF.

II. Methodology

The following chapter catalogs experimental design and biomolecular techniques implemented in this thesis.

a. Incremental Drug Induction and Mice Blood Pressure Monitoring

Kidney's autoregulation ability precludes drastic change in blood pressure from occurring in an acute manner; nonetheless, changes to baseline blood pressure can be visualized upon longitudinal monitoring. The following section discusses non-invasive blood pressure monitoring technique and chronic drug infusion methodology that allows for analysis of longitudinal effects of NMDA inhibition on blood pressure phenotype. Experimental cohort consisted of male and female mice from LS strain.

a. i. Osmotic Minipump Implantation

In order to infuse daily dosage of a drug continuously rather than acute injection of high dose, special devices named osmotic minipump were surgically placed in the animal cohort (Figure 6); the device systematically infuses a subcutaneous dose of the drug each day for 28 days. Proper drug concentration to be filled in each device was calculated based on the corresponding animal's weight (see Pharmacological Interventions). The minipump mechanism of action relies on an osmotic swell that increase the pump's internal pressure, thereby pushing the drug to be delivered continuously through a flow moderator (Figure 6).

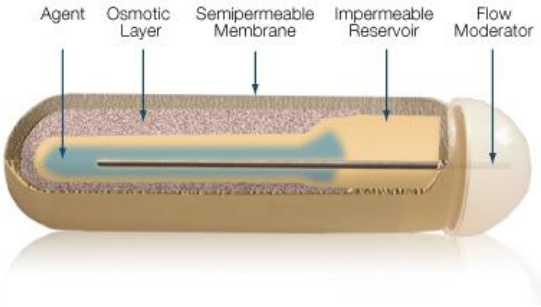

Figure 6: Apparatus of ALZET Osmotic Pumps. Image acquired from ALZET® Osmotic Pumps webpage.

Prior to minipump implantation, the animals were put under sedation via inhalation anesthesia. Animals were anesthetized with administration of isoflurane at 4%, which was then maintained at 1.75% isoflurane in oxygen throughout the procedure upon completion of initial induction. Depth of anesthesia and proper sedation was monitored throughout the procedure via assessment of lack of response upon a paw pinch, as well as constant respiration rate at 60 min^{-1}. Afterwards, incision was made to the dorsal aspect of neck, and dull-end surgical scissors was used to carefully widen the incision under the skin. The drug (or vehicle)-filled

minipump device was placed deep within the pocket, and incision site was sutured subsequently. Each animal was given buprenorphine SR 0.5 mg/kg for analgesia and was placed back in the cage for recovery. Postoperative monitoring was performed daily for days according to Emory's Animal Welfare Policies.

All drugs used in this thesis were commercially available except the GluN2C antagonist DQP997-74, which was provided by Dr. Stephenson Traynelis from the Department of Pharmacology, Emory University School of Medicine. The non-competitive, non-selective inhibitor MK801 (Sigma-Aldrich) dose used was 0.5 mg/kg/day dissolved in 10% DMSO-saline to do subcutaneous infusion using minipumps. The MK801 0.2mg/kg was dissolved in 0.5% ethanol-saline for the intraperitoneal injection. DQP997-74 was used on does 5 mg/kg/day diluted in 10% DMSO.

a. ii. BP-2000 Blood Pressure Analysis System

Real time blood pressure of mice can be measured through utilization of the tail cuff method using Visitech BP-2000 Blood Pressure Analysis System. Mice are placed on a warm platform and restrained by an individualized cubical chamber that is magnetically secured to the platform. The blood pressure cuffs are then positioned on the tails of the mice, and the ends of their tails are consolidated to the apparatus by masking tapes—excessive movement had to be minimized to promote a more accurate pressure reading (Figure 7). The Visitech BP-2000 uses transmission photoplethysmography, in which variations in the amount of light transmitted through the tail is detected as basic signal that is analyzed to determine the blood pressure and pulse rate. There was a 15-minute waiting period between completion of the set-up and initiation of pressure reading; in doing so, mice are able to become acquainted with the platform and the chamber, thereby lessening the stress factor from impacting the blood pressure measurement. The pressure measurement is initiated subsequent to the waiting period. The measurement consists of 5 initial pre-reading followed by 10 trials; the initial readings help the animals become acquainted with the process of blood pressure measuring, which in turn improves the quality of the subsequent 10 trials. The pressure measurement is recorded as the average of the 10 trials.

Figure 7: Apparatus of Visitech BP-2000 tail cuff system. Mice are placed on a heated platform which prevents thermal vasoconstriction, and their tails are taped to minimize excessive movement. Image acquired from University of Bath "How genes and environment in early life impact on adult health" webpage.

Even with the precautions mentioned above, mice blood pressure readings can have high variability depending on the condition of the animals on a given day. Consequently, we had to oblige with strict monitoring schedule for blood pressure monitoring. Upon initiation of the blood pressure monitoring protocol, each cohort are given a week of training period consisting of three non-adjacent measurement days (i.e. Monday, Wednesday, Friday, or Tuesday, Thursday, Saturday). Excessively frequent measurement schedule may induce stress, which can then correspond to alteration of blood pressure. Another factor that may erratically impact blood pressure is potential stress from merely moving the cages from animal room to the blood pressure room, as the cage carts and the elevator often generate unpleasant noises. To minimize variability from such causes, we measured the cohorts in different order from one day to another. Additionally, each animal was placed on the platform in a randomized order; the individual tails were marked with different number of stains to track which animal corresponded to which slot.

Subsequent to the training week, basal blood pressure was collected prior to the Osmotic Minipump implantation as delineated in the previous section. After 2-day recovery period, blood pressure was monitored throughout the duration of the minipump activity.

b. Localization and Quantification of NMDA Expression

Insight on NMDA expression is critical for evaluation of its physiological contribution to blood pressure phenotype. The following chapter discusses implementation of various biomolecular techniques in exploring expression of specific subunits of NMDA along the nephron in context of both kidney gene transcription and protein translation, as well as its localization to either cortical or medullary region within the kidney tissue. 129/SV background (Taconic) mice—the same background as the LS strain mice—were used alongside the experiments as control group, and Grin2C-KO (GluN2C knockout) strain were used for negative control. Both male and female mice of either LS or Taconic strain were implemented to evaluate sex difference simultaneously.

<u>b. i. RNAscope Imaging</u>

RNAscope is a cutting-edge biotechnology that involves detection and quantification of RNA molecules of interest via in-situ hybridization (ISH).[28,29] This technique is similar to the widely implemented immunofluorescence technique, which utilizes antibodies with attached fluorophores against proteins of interest, thereby allowing for visualization of a certain gene expression level; nonetheless, unlike conventional IF, RNAscope allows for evaluation of the transcription level. Correspondingly, co-implementation of RNAscope with conventional IF technique permits a more thorough insight in context of central dogma.

RNA molecules are known to auto-degrade very easily, as the hydroxyl group attached to carbon 2 of the ribose acts as a nucleophile that attacks the phosphate group of the RNA backbone (Figure 8). Consequently, it is particularly difficult to utilize RNA as a target

molecule in context of ISH. To overcome such a challenge, RNAscope implements a unique Z-shaped probe design (Figure 9a)— each Z probe contains about 18 to 25 base pairs that can bind to different segments of the RNA molecule[28]; the probe is correspondingly able to hybridize to smaller segments of the target RNA molecule, which somewhat negates the rapid auto-degradation of the mRNA. On the contrary, signal development requires "double Z" binding, where two independent Z-shaped probes must hybridize to the target sequence in an adjacent manner in order for fluorescence amplification to occur (Figure 9b). Such probe design minimizes non-specific signal production, as it is highly unlikely that two erroneous binding occurs consecutively.

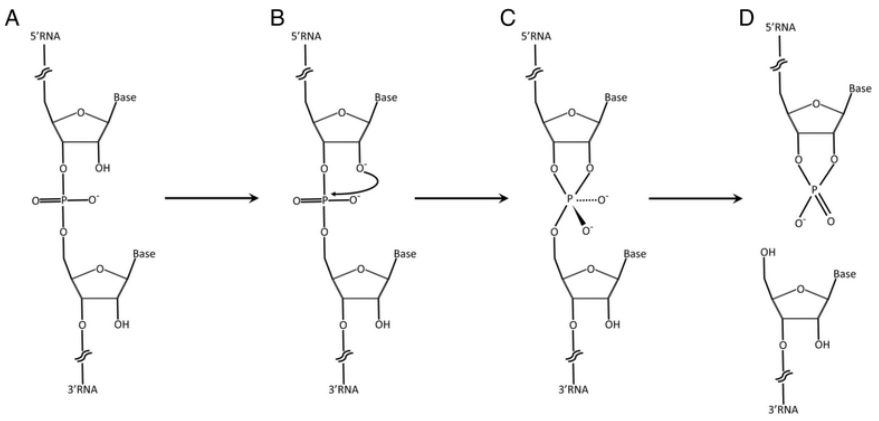

Figure 8: Schematics of RNA auto-degradation mechanism. Image obtained from "Alkaline hydrolysis to remove potentially infectious viral RNA contaminants from DNA" Lemire et al., ResearchGate webpage.

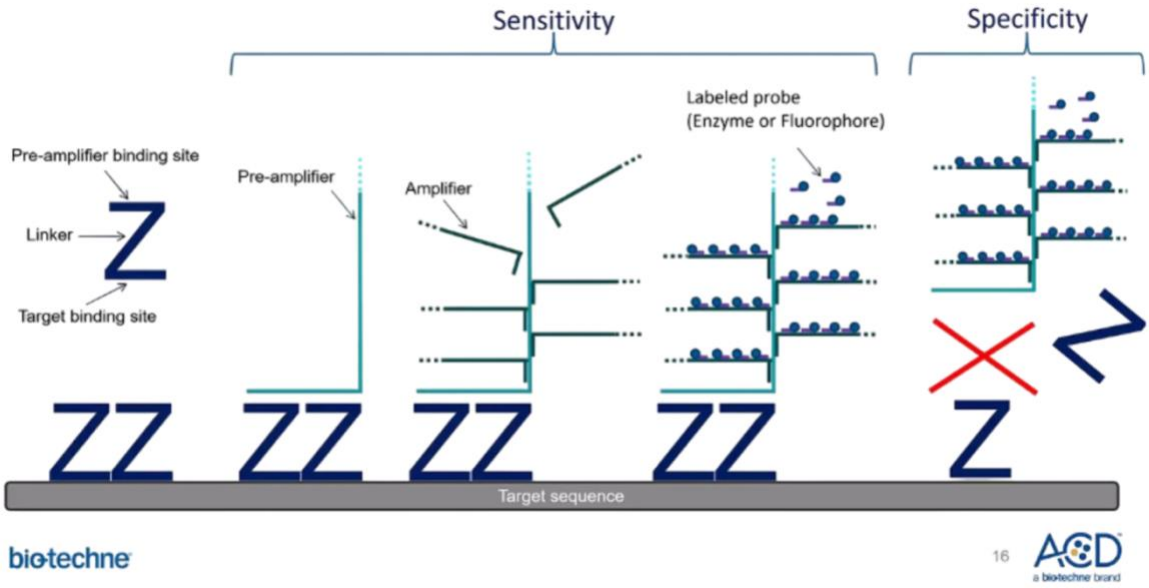

Figure 9: RNAscope assay design. Z-shaped probe detects short segments of target mRNA sequence, and signal amplification occurs solely upon binding of two Z-probes in an adjacent manner. Image obtained from Advanced Cell Diagnosis (ACDbio) RNAscope product webpage.

Even though RNAscope assay is designed to circumvent limitations from instability of mRNA molecules, the entirety of experimental protocol must be strictly monitored and controlled for proper imaging results. Through multiple trial and error, we were able to develop an optimal timeline for the RNAscope experiment. Fresh mice kidneys were harvested via anesthetized excision surgery. Each organ harvested were immediately consolidated to a plastic case filled with Optimal Cutting Temperature (OCT) compound. The cases were then stored in -80 °C freezer until further processing. The consolidated organ must be stored for approximately 24 hours; shorter freezing period will result in suboptimal processing, while prolonged storage will result in degradation of the RNA molecules even in considerably low temperature as -80 °C. After the freezing period, the tissues were added onto the microscope slides via Thermo Scientific Cyrobar machine. Each section was prepared to be 6 μm in thickness—we encountered issue of thicker tissue section easily washing away during the experimental protocol. Upon embedment of the tissue, the slides were immediately placed in an isolated case; the case itself was kept within dried ice to ensure a moderately cold temperature throughout. Once all slides were prepared, the case was stored in -80 °C freezer for approximately 24 hours. Such timeframe allowed for the OCT compound to completely adhere to the glass surface of the slide, which once again prevents the tissue section from washing away.

Subsequently, the slides with frozen tissue sections were removed from the -80 °C freezer, thawed for approximately 30 seconds, and immediately placed in 4% paraformaldehyde solution at 4 °C for tissue fixation. The fixation step allows for preservation of tissue structure and prevention of cellular destruction. After 1 hour incubation in the refrigerator, the slides were placed in increasing concentration of ethanol solution—50%, 70%, and 2x 100% respectively, each for 5 minutes at room temperature (RT). The step completely dehydrates the tissues, which further contributes to proper fixation of the samples. The samples were air-dried for 10 minutes, while which border was drawn with ImmEdge Hydrophobic Barrier Pen around the tissue—the hydrophobic barrier allows for application of a few drops of reagents to the tissue of interest without the need to submerge the entire slide in a solution. The slides were then placed in humidity control tray to be incubated with hydrogen peroxide for 10 minutes at RT. The incubation was followed by wash step (2 minutes at RT x2 in phosphate-buffered saline (PBS) solution) then additional 30-minute incubation with Protease IV reagent provided in the RNAscope assay kit. The steps induce degradation of various proteins that may be bound to the target mRNA molecule, thereby permitting a more comprehensive detection of the RNA.

Probe against Grin2C (gene corresponding to GluN2C) mRNA was prepared during incubation steps described above. The probe and probe diluent (both provided in the RNAscope assay kit) were removed from the fridge and warmed to 40 °C via water bath. Afterwards, both reagents were chilled to RT for approximately 10 minutes. The probe was prepared in 1/50 dilution ratio and was briefly centrifuged. Upon completion of incubation step with Protease IV reagent, approximately 50 μL of the prepared probe was added to each sample.

The entire humidity control tray was then placed in an incubation oven set to 40 °C for 2 hours. After probe hybridization, the signal was amplified using the following reagents, as provided in the RNAscope assay kit: AMP I, 30 minutes at 40 °C; AMP II, 30 minutes at 40 °C; AMP III, 15 minutes at 40 °C; HRP-C2 signal developing reagent, 15 minutes at 40 °C. Subsequent to each incubation step, wash step (2 minutes x2 at RT) with 1x wash buffer as provided in the RNAscope assay kit was incorporated.

Opal 690 dye was prepared during the signal amplification steps described above; the dye was warmed to RT and diluted in tyramide signal amplification buffer reagent (provided in the RNAscope assay kit) in 1/750 dilution ratio. In order to protect the validity of the fluorophore, all protocol from here on out was conducted in the dark and the Eppendorf tube containing the diluted dye was wrapped with aluminum foil. Upon application of approximately 50 μL of the dye to each tissue, the humidity control tray was once again placed in 40 °C incubation oven for 30 minutes. Subsequently, blocking reagent was applied to each sample (15 minutes at 40 °C); the step reduces non-specific signal development, thereby improving the overall quality of the imaging results. Finally, DAPi nuclei counterstaining reagent was applied for 30 seconds at RT, which was quickly followed by slide mounting step with AquaMount mounting medium and 1"x1" mounting glass. The slides were refrigerated at 4 °C in a dry, dark chamber until microscope evaluation in the subsequent day.

The mounted slides were evaluated under Confocal Microscope, 200x magnification. Channel with wavelength λ = 405 nm were utilized to detect DAPi nuclei counterstaining, while channel with wavelength λ = 633 nm corresponded to the Opal 690 red fluorescent dye. Four images were obtained from each slide, encompassing four different quadrants of the tissue—in the process, both cortical and medullary region were captured. The images were then uploaded to quantification software named QuPath V0.5.1 (University of Edinburgh) for data analysis. Strength of the fluorophore was adjusted accordingly via minimum detection threshold. Because RNAscope signal is often observed as spots, called puncta, in cells, we first performed a cell deconvolution to determine Subcellular Component Detectionto quantify the signaling within the given image. The data was generated as either Puncta (number of separable points) or Cluster (aggregation of multiple puncta) per area in μm^2. Each puncta represent an mRNA molecule, and a cluster is defined by when more than 5 puncta are detected together within the context of pixel size. The whole tissue section was analyzed accordingly.

b. ii. Immunofluorescence

Immunofluorescence (IF) imaging involves utilization of fluorophore-tagged antibodies that bind to the protein of interest; as a result, implementation of conventional IF alongside RNAscope allows for a comparative analysis in rate of translation versus transcription of the given protein. We used indirect antibody binding method, where primary antibody binds to the protein of interest and secondary antibody with attached fluorophore binds to the primary antibody (Figure 10). NeuroMab anti-GluN2C antibody (Appendix c.) were used as primary antibody, followed by goat anti-mouse secondary antibody with fluorophore at $\lambda = 633$ nm.

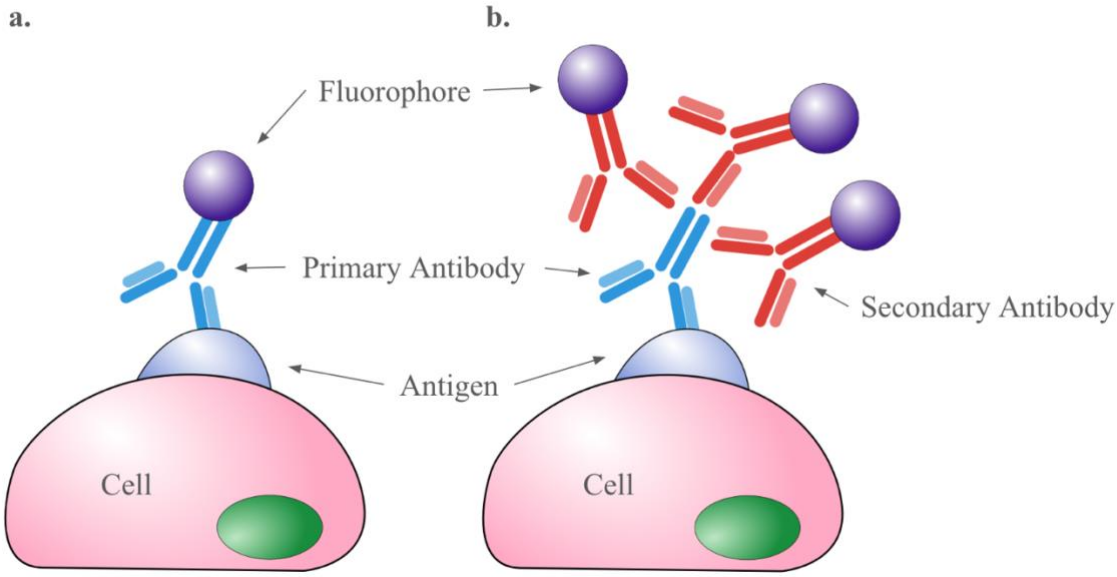

Figure 10: Schematics of direct versus indirect antibody binding. (a.) Direct antibody binding: fluorophore is directly attached to primary antibody that binds to target antigen. (b.) Indirect antibody binding: primary antibody binds to target antigen, and secondary antibody with attached fluorophore binds to the primary antibody. (Figure generated by Joy H. Lee)

Frozen tissue sections were removed from the -80 °C freezer, thawed for approximately 30 seconds, and immediately placed in 100% acetone solution at 4 °C for tissue fixation. The slides were then washed with phosphate-buffered saline + 0.1% Tween solution (PBS-t) for three minutes at RT x3. Afterwards, hydrophobic border was drawn with ImmEdge Hydrophobic Barrier Pen. This step is similar to that of RNAscope protocol, but it is of vital importance to keep the samples moist at all times because the tissues have not undergone the same fixation and dehydration procedure as mentioned in the RNAscope protocol. The samples were then placed in the humidity control tray and was blocked with 1% Albumin solutions for 20 minutes at RT. Approximately 50 µL of primary antibody in 1/100 dilution were added to each sample subsequent to the blocking step, and the slides were incubated at 4 °C overnight.

On the following day, the slides were incubated with secondary antibody in 1/400 dilution for 2 hours at RT. Similar to RNAscope protocol, all procedure from here on out were conducted in the dark in order to protect the validity of the fluorophore. The slides were once again washed with PBS-t solution for three minutes at RT x3 before DAPi nuclei counterstaining and slide mounting. Counterstaining and mounting protocol was identical to that of RNAscope slide mounting described in the previous section.

Once again, the mounted slides were evaluated under Confocal Microscope (Leica), 200x magnification. Channel with wavelength λ = 405 nm were utilized to detect DAPi counterstaining, while channel with wavelength λ = 633 nm corresponded to the secondary antibody with signal of interest. The imaging results were then uploaded to QuPath V0.5.1 (University of Edinburgh) for quantification. Nonetheless, protein detection signal is displayed diffusely along the cell membrane unlike that of RNAscope. As a result, the signal was quantified by means of number of positive cells, rather than evaluating subcellular components.

c. Evaluation of Renal Blood Flow and Autoregulatory Mechanism

The following section delineates additional experimental procedures that can provide insight on specific physiological mechanism between NMDA receptor inhibition and blood pressure phenotype. We specifically focused on two crucial aspects of kidney functionality—RBF and autoregulatory mechanism evaluation.

Male LS mice were put under sedation via inhalation anesthesia. Animals were anesthetized with administration of isoflurane at 4%, which was then maintained at 1.75% isoflurane in oxygen throughout the procedure upon completion of initial induction. Depth of anesthesia and proper sedation was monitored throughout the procedure via assessment of lack of response upon a paw pinch, as well as constant respiration rate at 60 min^{-1}. Animals were kept normothermic via utilization of thermal-controlled surgical pad. Afterwards, an incision was made to the animals' neck, which exposes their carotid arteries. The left carotid artery was then carefully micro-dissected and isolated from the vagus nerves and jugular vein—microscope was used for careful manipulation, as rupture of carotid artery would lead to death within minutes. Upon isolation, small catheter (p10) was inserted into the artery. Either ends of the segment at which the catheter would be inserted was tied to prevent excessive bleeding. Upon successful insertion, the catheter was consolidated in place with a third knot. The catheter allows for real-time monitoring of blood pressure while keeping the animal alive through the duration of the procedure.

Second incision was made to the animals' left lumbar region in order to expose the kidney. A small needle laser doppler probe was inserted into the kidney via utilization of micromanipulator for precise positioning. Upon visualization of proper placement, the probe

was fixed with Vetbond tissue adhesive to minimize movement artifacts during data collection. The probe was positioned at the renal cortex to ensure accurate real-time monitoring of RBF.

Subsequent to the surgical preparation as delineated above, a 30-minute stabilization period was allotted for the animal to acclimate to the setup, during which RBF and central blood pressure were continuously recorded; the data served as baseline data, which ensures steady-state conditions (Figure 15). After the stabilization period, a single intraperitoneal (I.P.) injection of MK801—a non-competitive, non-selective NMDA inhibitor— (0.2 mg/kg) diluted in 0.5% ethanol-normal saline was administered. RBF and central blood pressure were recorded again for 30 minutes post-injection. Data collection was performed in 10-minute intervals, and RBF was quantified in arbitrary renal blood flow units (BFU) that were equivalent to millivolts. Additionally, we calculated the renal vascular resistance by dividing mean arterial pressure over RBF, expressed as mmHg/BFU

c. i. Spectral Analysis

To assess renal blood flow oscillations, spectral analysis was performed via LabChart Spectra Function (AD Instrumets). Data was processed using a Fourier transformation, with a 1006 K-point dataset and a 50% overlap to optimize frequency resolution. A 500 mHz low-pass filter was applied to minimize noise, and power density was quantified across different frequency bands. The power density in specific frequency bands associated with renal autoregulatory mechanisms (i.e. CNTGF and TGF) was analyzed. Spectral peaks corresponding to CNTGF (0.08 Hz), TGF (0.1-0.5 Hz), and neurogenic components (0.01-0.05 Hz) were identified and comparatively scrutinized prior and subsequent to MK801 injection. Data was averaged over 10-minute periods for analysis, and all values were expressed as average ± SEM.

d. Data Analysis

Data were collected and expressed as mean ± standard deviation (SD), and p-value < 0.05 was considered statistically significant. The choice of statistical tests varied based on the experimental design and data distribution, ensuring that appropriate statistical assumptions were met.

For the longitudinal analysis of acute and subacute blood pressure changes following administration of MK801 and DQP997-74, simple linear regression was used to compare slopes between the intervention and vehicle groups using the F-statistic. Due to the presence of two distinct longitudinal patterns with a clear breakpoint on day seven following acute MK801 infusion, the data were analyzed using two separate linear regression models. This approach was justified based on improved goodness-of-fit compared to a quadratic or polynomial regression model. In the salt sensitivity experiment, longitudinal data were analyzed using multiple unpaired t-tests with Bonferroni correction. Due to clear observable

sex interaction effect during data processing, animals in these experiments were stratified by sex.

As for GluN2C RNA and protein expression levels and blood pressure in knockout mice, a two-way ANOVA was performed with sex and genetic background as factors, as well as Tuke's multiple comparison test. Paired t-tests were used to compare renal blood flow (RBF) before and after MK801 infusion, as well as for power density comparisons between spectra.

III. Results

a. Acute and Subacute Effect of NMDA Inhibition on Blood Pressure Under Normal Salt Diet

To evaluate the effect of NMDA receptors on blood pressure (BP), we measured BP using BP-2000 tail cuff method prior and subsequent to infusing either non-selective NMDA inhibitor MK801 or vehicle (10% DMSO) in mice fed with regular chow (normal salt diet, NaCl 0.4%). Both males (n=4) and females (n=4) LS mice were subcutaneously infused with corresponding drugs for 14 days using Osmotic minipumps. As demonstrated in Figure 11a, MK801 treated mice experience an increase in blood pressure comparted to the vehicle counterpart after seven days of infusion (SBP 130.2 ±14 vs. 104.3±17 mmHg, β=1.33 vs 1.116, $p<0.01$). Nonetheless, BP seemingly normalized during the subsequent week (day 7 to 14) of infusion, with no statistically significant difference between the two groups (116.8±6 vs. 119.8±9 mmHg, β=1.3 vs 0.92, $p=0.09$). When results were stratified by sex (Figure 11b), the same longitudinal changes were observed—the same acute increase and subacute normalization occurred in both sexes subsequent to infusion of MK801. Furthermore, such results indicate that, under normal salt diet, infusion of MK801 induces a dual-phase effect: acute increase in blood pressure in the first seven days post-op, and normalization to basal level by day 14 among LS mice. Such change is observable in both male or female cohort, and correspondingly difference in sex is not statistically significant.

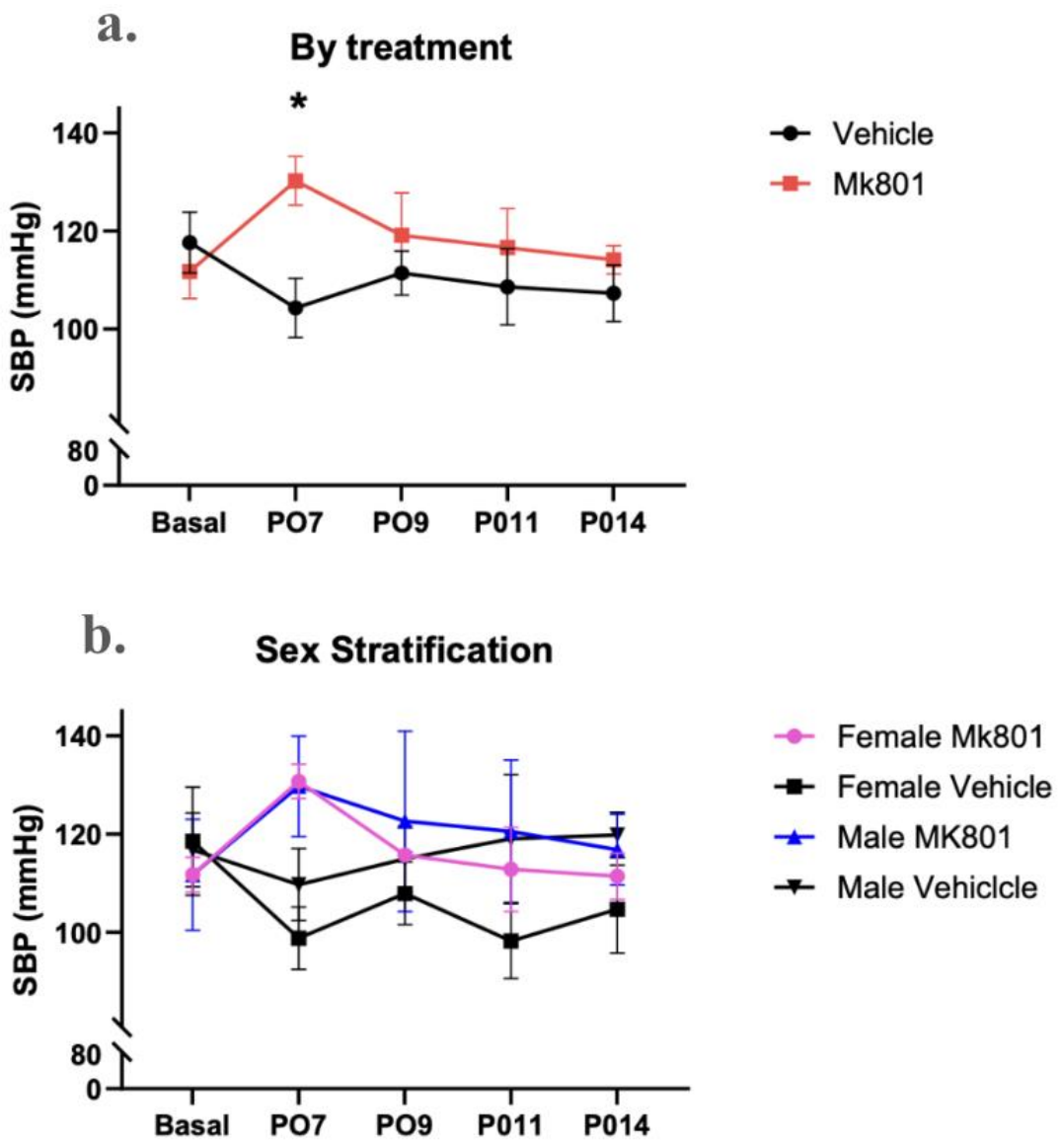

Figure 11: Infusion of MK801 induces acute increase in systolic blood pressure (SBP) in LS mice. (a.) LS mice on normal salt diet exhibit elevated postoperative SBP until day seven ($p<0.01$), then stabilizes to basal level comparable to vehicle group. (b.) Both male and female LS mice display such pattern, with statistical significance being more apparent in the female cohort *$p<0.01$, n=8

b. MK801 Prevents Salt Sensitivity in male Liddle Syndrome Mice

In order to uncover the potential mechanism responsible for the dual-phase effect as delineated in previous section, we evaluated the BP response to MK801 upon placing the animals on high salt (HS) diet (NaCl 4%). Since LS animals easily develop HTN upon excess sodium intake, we speculated that the postoperative BP increase over the first week observed in the previous experiment would not be readily observable, due to the pressure-natriuresis mechanism already in action. We instead hypothesized that BP would acutely decrease upon NMDA inhibition secondary to its inhibitory effect on ENaC, as observed in the second phase (subacute) of normal salt diet cohort; such phenomenon would result in decreased salt reabsorption and corresponding normalization of the blood pressure. As demonstrated by Figure 12a and b, there was evident sex difference in salt-sensitivity, where female did not display increase in blood pressure despite HS diet (two-way ANOVA interaction for sex and treatment, $p < 0.01$). The data was correspondingly stratified and analyzed by sex.

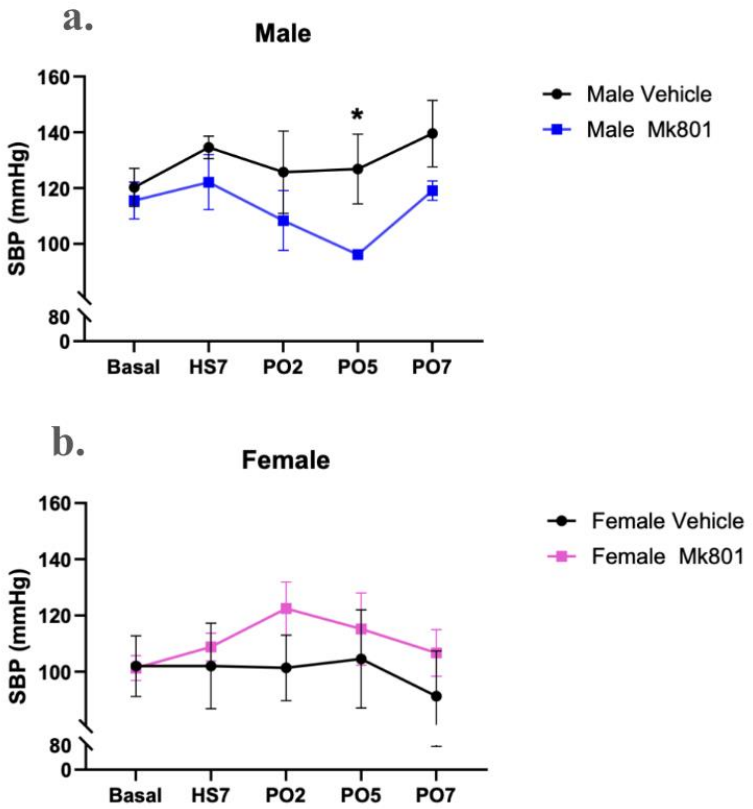

Figure 12: SBP trend of LS mice on HS diet. (a.) Male LS mice exhibit an increase in SBP on high salt (HS) diet. Upon MK801 infusion, SBP acutely decreased, most prominently noted on day 5 ($p<0.001$). (b.) Female LS mice do not exhibit observable change in blood pressure in response to high salt diet. Upon MK801 infusion, female LS mice do not display statistical significance in alteration of blood pressure.

Male LS mice display salt-sensitivity, showing increased blood pressure upon placement on HS diet—correspondingly, the male cohort was at an elevated blood pressure level in comparison to the female cohort at the time of osmotic minipump implantation surgery (Figure 12 a and b). Female LS mice did not display salt-sensitivity, contrary to our initial hypothesis. Postoperatively, male LS mice on HS diet infused with MK801 (n=5) display an acute decrease in blood pressure, most prominently observed by day five post-operation (SBP 96.1±2.5 vs.

126.8±25, p<0.001) (Figure 12a). Vehicle group on HS diet (n=5) displayed HTN throughout the course of the experiment. Sex difference is apparent in this cohort, as only male LS mice seemingly exhibited such change in blood pressure phenotype. Female LS mice did not develop observable changes to blood pressure in response to MK801, despite displaying a transient increase after the second day of infusion that reflects the observation in normal salt diet cohort.

c. GluN2C Subtype Receptor on Blood Pressure Regulation.

c. i. DQP997-74 GluN2C-Specific Inhibitor

To explore which NMDA subtype channel may be implicated in blood pressure regulation, we utilized a newly developed selective, brain impenetrant, GluN2C antagonist (DQP997-74) in order to evaluate implications of variance in NMDA receptor subtype on observable changes to blood pressure. Basal blood pressure was measured preoperatively, and the experimental protocol as delineated above was implemented with osmotic minipump containing either DQP997-74 in place of MK801 or saline. Male and female LS mice were divided to either experimental (n=3) or vehicle group (n=3), and any notable sex difference was noted accordingly.

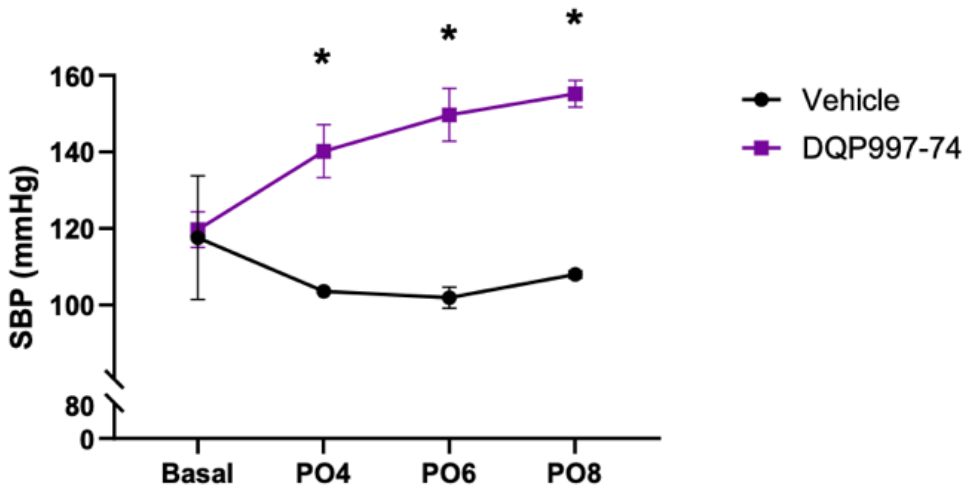

Figure 13: Effects GluN2C antagonist on LS mice SBP. Subsequent to infusion of DQP997-74, LS mice on normal salt diet develops postoperative increase in SBP that is statistically significant in PO4, PO6, and PO8 (p=0.001). Such phenomenon closely reflects results from MK801 normal salt diet cohort, as demonstrated in Figure 12.

Similar to MK801 treated on normal salt diet cohort, LS mice infused with GluN2C antagonist DQP997-74 exhibits increase in postoperative blood pressure compared to baseline. The magnitude of increase in blood pressure is a significant comparatively, average SBP on day eight post-operation reaching 155.2±6 vs 108±1.6 mmHg, P=0.008 (DQP997-74 vs.

vehicle), with a longitudinal slope for the DQP997-74 treated group of β=1.32 vs.β=0.87 for vehicle (p=0.001)

c. ii. RNA and Protein Expression

To further explore the role of GluN2C, we evaluated the expression of the channel subunit in the kidney. We utilized RNAscope ISH to evaluate RNA transcription level, and conventional immunofluorescence technique with microscopy analysis to quantify protein abundance. By comparatively quantifying both mRNA and protein level within the same animal, we are able to gain better insight on regulation of the gene expression in context of central dogma in LS mice. Kidney was harvested from male and female LS mice (n=3) alongside their Taconic (WT) counterpart (n=3). Multiplicate of tissue slides used in both experiments; since proteins are known to be much more stable than mRNA molecules, IF experiment was done subsequent to RNAscope.

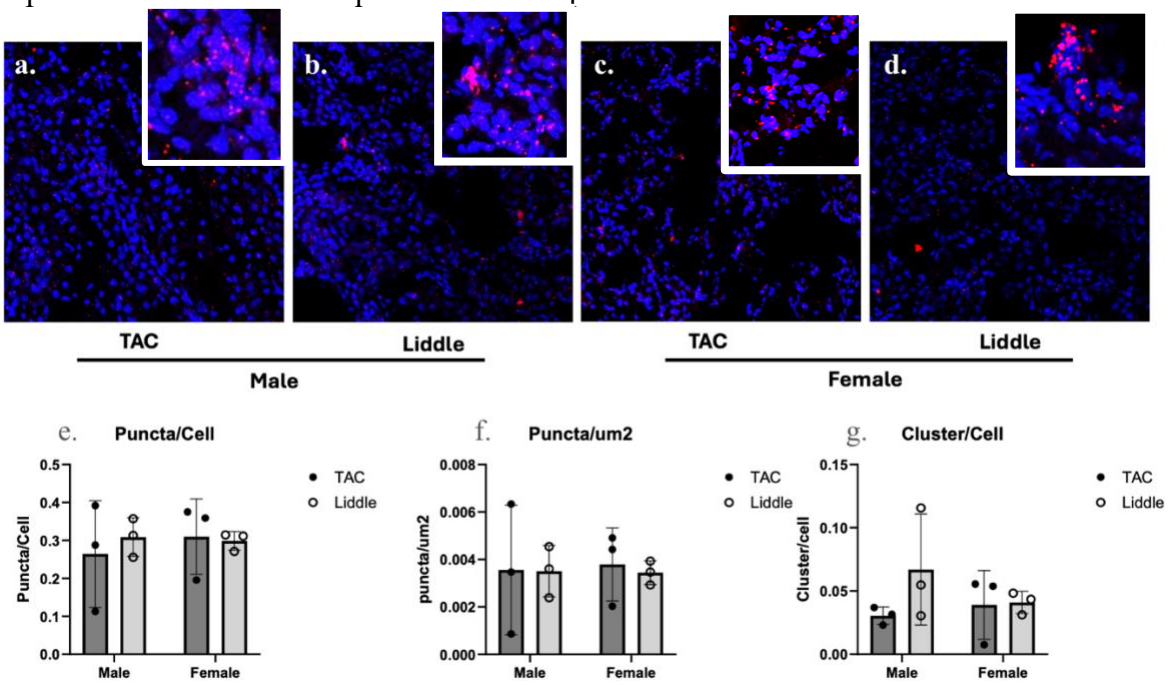

Figure 14: GluN2C RN transcription in kidney. RNA molecules were found in wild type and LS mice and in both male and female, no notable difference between genetic background or sex was observed. (a.) Taconic male Grin2C mRNA signal detection. (b.) LS male Grin2C mRNA signal detection. (c.) Taconic female Grin2C mRNA signal detection. (d.) LS female Grin2C mRNA signal detection. (e.) Quantification of Grin2C signal in terms of # puncta/# cells. (f.) Quantification of Grin2C signal in terms of # puncta/area (μm^2). (g.) Quantification of Grin2C signal in terms of number of # cluster per # cells. Leica 200x magnification.

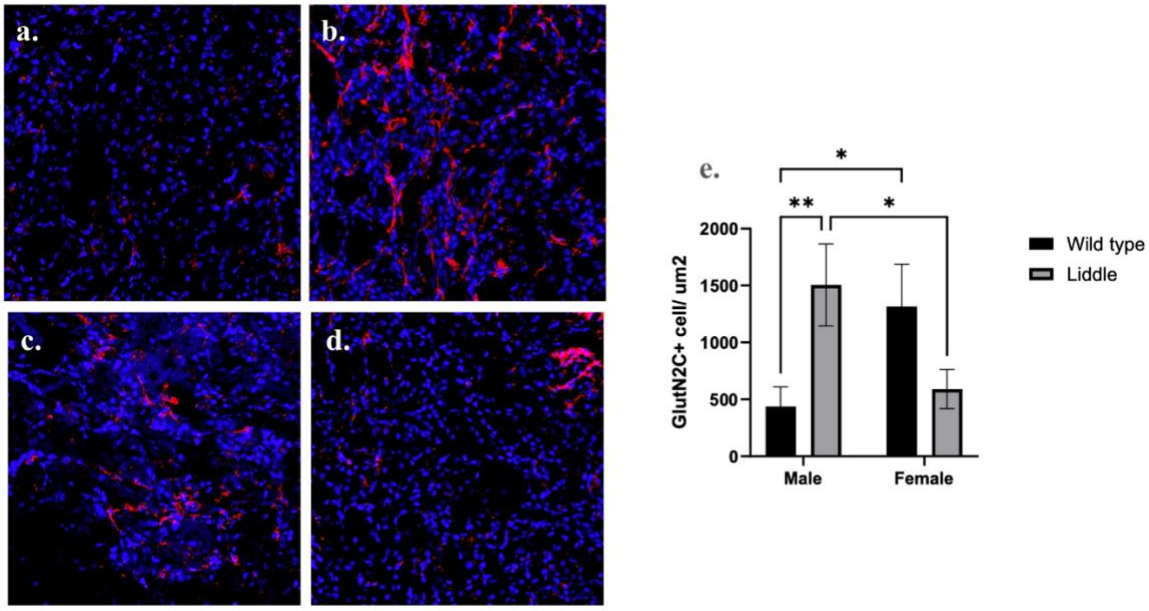

Figure 15: GluN2C Immunofluorescence (IF) Imaging results and quantification. Protein abundance evaluated by positive cells per area reveled sex and background interaction. In wildtype animals, female have a significant higher protein abundance, whereas in Liddle syndrome the relationship was inversed; male have the highest level of GluN2C, almost three time to the wild type males. (a.) Taconic male GluN2C protein signal detection. (b.) LS male GluN2C protein signal detection. (c.) Taconic female GluN2C protein signal detection. (d.) LS female GluN2C protein signal detection. (e.) Quantification of GluN2C signal as # GluN2C-positive cells/area (μm^2) *$p<0.05$ **$p<0.01$ Leica 200x magnification.

As observed in Figure 14, results from the RNAscope experiment demonstrate that there is no statistically significant difference across genetic strain or between male and female when analyzed as either Puncta per Cell, Puncta per μm^2, or Cluster per μm^2. Additionally, there appears to be high variability in strength of the signal within the same cohort, which increases standard deviation considerably. Such results corroborate the null hypothesis that there is indeed no difference in quantity of Grin2C transcription between WT and LS strain, and between male and female.

On the other hand, results from IF experiment demonstrate that there is indeed statistical significance in differences of protein level across all cohorts (Figure 15). Taconic males showed significantly less signaling compared to male LS cohort (437.3±172.3 vs. 1506±360, $p<0.01$), while the females displayed apparent reciprocal results (Taconic female 1316±371.8 vs 590±172.5 $p=0.05$). Additionally, there is apparent sex difference in both Taconic and LS strains; Taconic females had considerably higher protein level compared to their corresponding male cohort ($p=0.02$), which is consistent with results from prior studies with C57 mice strain (Supplemental data). Interestingly, the relationship was inversed in case of LS cohorts, where

males have the higher GluN2C level (p=0.02). The discrepancy between RNAscope and IF results suggest potential post-transcriptional regulation.

c. iii. Blood Pressure on Grin2C-KO Mice

To corroborate the role of the GluN2C subunit in BP regulation, we evaluated the BP of Grin2C-KO (knock-out of gene that encodes GluN2C subunit) and Grin2D-KO (knock-out of gene that encodes GluN2D subunit) strain in comparison with black C57b6 wildtype mice (n=5) via tail cuff method under normal salt diet versus HS diet. The pressure was measured at three different days and averaged after completion of three training sessions over a week.

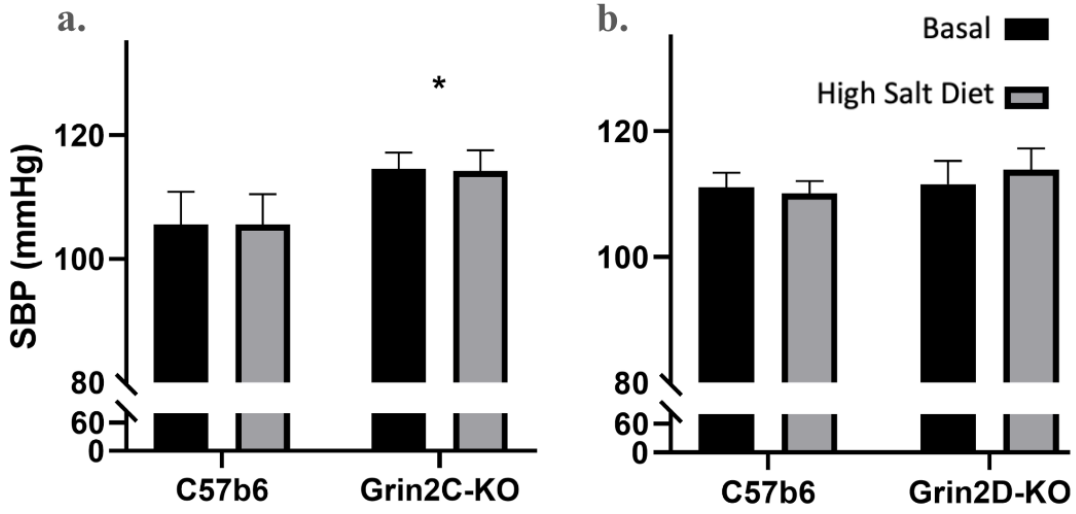

Figure 16: Basal blood pressure and high salt diet effect in Grin2C-KO. (a.) Grin2C-KO cohort has higher systolic blood pressure (SBP) in comparison to the C57 wildtype, displaying statistical significance ($p<0.01$). (b.) Grin2D-KO cohort displays no notable difference compared to WT counterpart. Either group did not display salt-sensitivity, as exposure to HS diet did not alter the blood pressure phenotype in any group.

As demonstrated in Figure 16, Grin2C-KO strain displays high basal blood pressure level in comparison to its WT counterpart. The average systolic blood pressure (SBP) for C57b6 mice was 105.6 ± 10.5 mmHg, whereas SBP on GluN2C-KO mice was 114.6 ± 7.3 mmHg ($p<0.01$). On the contrary, SBP of Grin2D-KO mice was 111.6±10.4 mmHg, showing no significant differences from the matched control (111.1±4.6 mmHg; p=0.93). These data indicate that GluN2C participate in BP regulation.

d. Implications of NMDA on Renal Blood Flow and Autoregulation

To investigate potential renal mechanisms associated with NMDA receptor inhibition, we examined renal blood flow (RBF) and the intrinsic autoregulatory mechanisms following the acute infusion of MK801 versus vehicle. Figure 17 demonstrates a representative tracing of

central blood pressure (red) and RBF (green) in LS mice. Subsequent to catheter implantation and the fixation of the laser Doppler flow probe, a 30-minute stabilization period was recorded before obtaining baseline measurements. Afterwards, an intraperitoneal (IP) bolus of MK801 was administered. BP and RBF were monitored for 30 minutes post-injection.

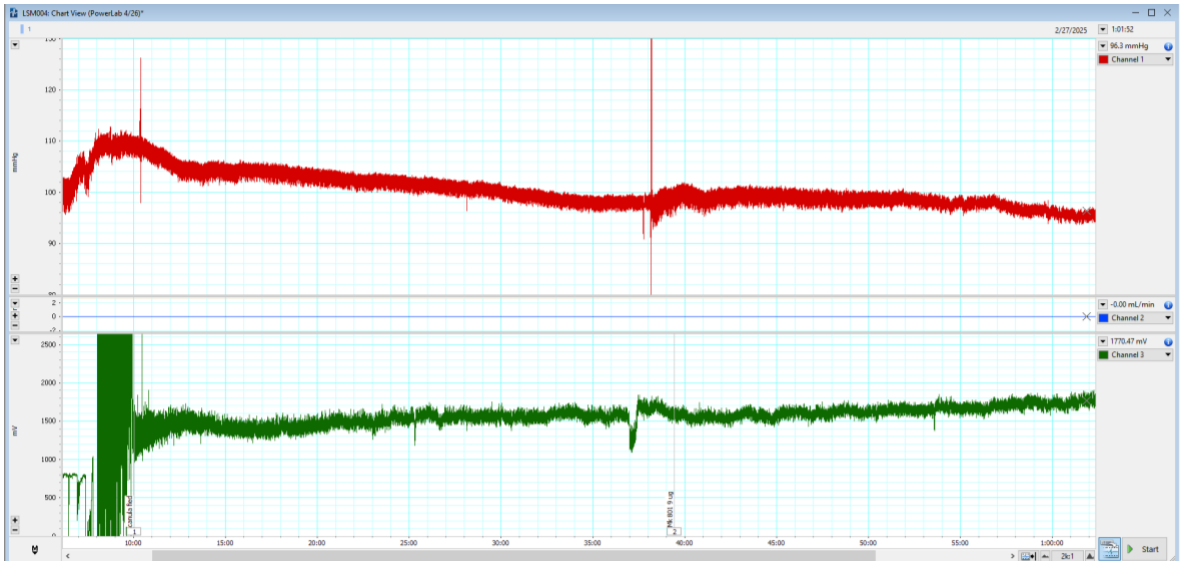

Figure 17: Real-time tracing of central blood pressure and renal blood flow. Blood pressure (red) and RBF (green) were recorded simultaneously, prior and subsequent to acute infusion of MK801.

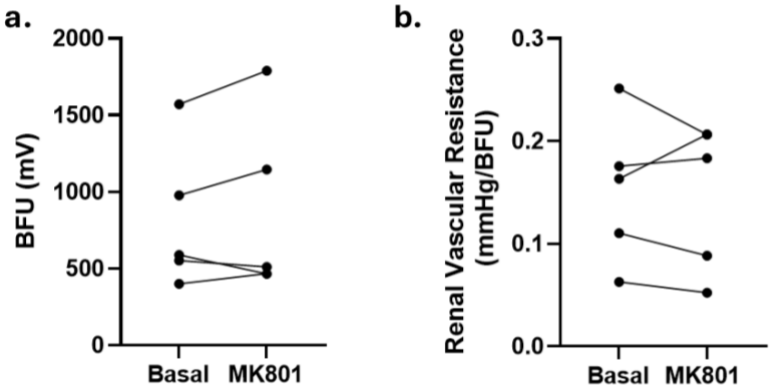

Figure 18: Change in blood filtration unit (BFU) and renal vascular resistance prior and subsequent to MK801 injection. No statistical significance was noted across either results.

As demonstrated in Figure 18, no significant difference in RBF were observable prior and subsequent to MK801 injection. (818.4±471 vs. 875.6±585.9 BFU, p=0.42 Basal vs. MK801 injection) Nonetheless, notable variability among animals were present, as some exhibited a decrease in RBF while others displayed no change or even transient increase. Consequently, we were unable to quantify a net change or draw transparent conclusions with usage of laser Doppler flowmetry alone. Analyzing renal vascular resistance, we found similar result with no changes prior and subsequent to MK801 (p=0.74)

Correspondingly, we performed spectral analysis using Fourier transformation to identify specific oscillation frequencies associated with connecting tubule-glomerular feedback (CNTGF) and tubuloglomerular feedback (TGF). As demonstrated by Figure 19, we observed a notable decrease in power density at 0.08 Hz (blue arrow) corresponding to CNTGF, subsequent to MK801 administration (0.22±0.1 vs 0.08±0.04, p=0.03). On the contrary, no significant changes were observed in the power density associated with TGF (0.1-0.3 Hz, orange arrow); such results corroborate an acute decrease in the vasodilator mechanism CNTGF in renal autoregulation following MK801 infusion. The relative contribution of each component (CNTGF and TGF) was analyzed using the CNTGF/TGF ratio, which displays overall reduction of the CNTGF component but without statistical significance (p=0.08) secondary to the high variability.

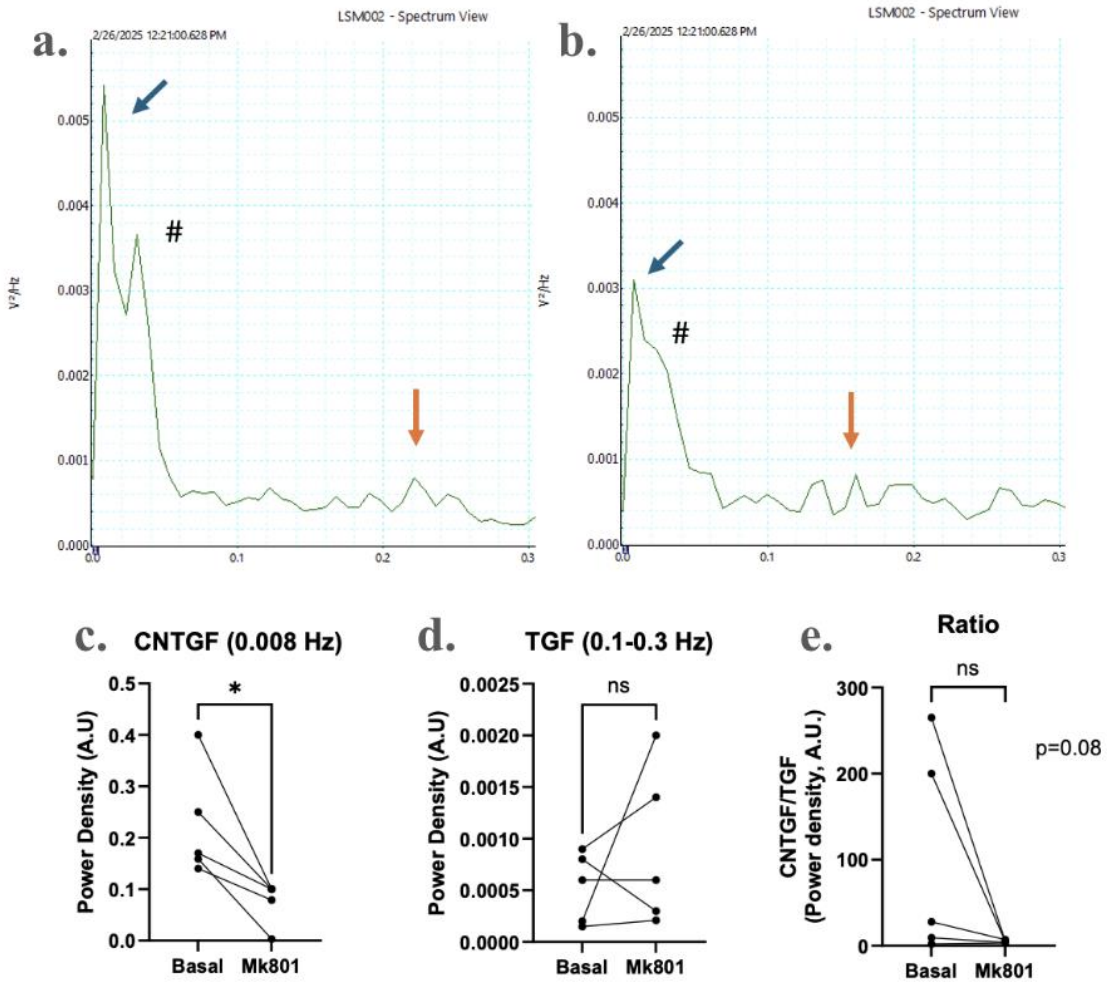

Figure 19: Fourier transformation of renal blood flow oscillation. (a.) Fourier transformation graph of oscillation prior to MK801 injection. Blue arrow indicates oscillation corresponding to CNTGF, and orange arrow indicates oscillation corresponding to TGF. (b.) Fourier transformation graph of oscillation subsequent to MK801 injection. Blue arrow

indicates oscillation corresponding to CNTGF, and orange arrow indicates oscillation corresponding to TGF. Pound symbol denotes neurogenic compound of RBF. (c.) Power density of CNTGF, which displays notable decrease subsequent to MK801 injection. (d.) Power density of TGF, which displays transient increase subsequent to MK801 injection but without statistical significance. (e.) Ratio of CNTGF to TGF power density.

Moreover, we noted the presence of a spectral peak in the range of 0.01–0.05 Hz, typically associated with a neurogenic component of RBF (denoted by pound symbol). Although this change was not quantitatively assessed, we observed a systematic decrease in this frequency band following MK801 administration. This reduction may potentially reflect a decrease in neurogenic tone, consistent with previous reports of MK801's effects on sympathetic nervous activity. Ultimately, these data demonstrate an intrinsic alteration in renal autoregulation subsequent to acute MK801 injection, but without a noteworthy net effect on total blood flow.

IV. Discussion and Conclusion

The main finding of this thesis is that NMDA receptors, specifically GluN2C, are involved in blood pressure regulation. We found compelling evidence that this effect is closely associated with alterations in renal autoregulation, particularly via connecting tubule glomerular feedback (CNTGF) inhibition. BP monitoring prior and subsequent to infusion of MK801 in LS mice demonstrates a paradoxical effect of NMDA receptors' function on blood pressure regulation as discussed in the introduction. Under normal salt diet condition, inhibition of NMDA seemingly elevates blood pressure in the first seven days post-operation; such phenomenon most likely relates to deactivation of connecting tubule glomerular feedback (CNTGF), which is mediated by ENaC upon detecting increase in Na^+ concentration in the connecting tubule under normal conditions.[30] Previous research demonstrates that *in vivo* NMDA agonist application induces increase in both CNTGF and ENaC open probability[23]; moreover, the use of NMDA inhibitors decrease ENaC activity and consequently CNTGF, and thus we can reasonably infer that NMDA inhibition would have an opposite effect, decreasing both CNTGF and ENaC activity. Decrease in CNTGF would induce vasoconstriction of afferent arteriole, which would impact glomerular filtration and renal perfusion.[13] We speculate that, unlike their WT counterpart, LS mice are typically much more vulnerable to development of HTN as a result of an exaggerated ENaC activity resulting in excessive Na^+ reabsorption and potential hypervolemia at baseline[25]; given that glomerular filtration rate (GFR) reduction correlates with decreased Na^+ excretion, this process may be especially critical LS mice, exacerbating the hypertensive phenotype.[31]

On the other hand, subsequent subacute decrease in blood pressure in days seven through 14 post-operations can be explained by decrease in ENaC activity itself. ENaC deactivation would alleviate the effects of excess Na^+ reabsorption secondary to gain-of-function mutation in LS mice. We speculate that ENaC deactivation would reduce the level of hypervolemia,

which would eventually lessen blood volume and thereby decrease blood pressure. Moreover, we can reasonably infer that alleviation of hypervolemia takes approximately seven days for it to surmount the acute increase in blood pressure secondary to CNTGF inhibition due presence of the pressure natriuresis mechanism, excretion of the excessive sodium deposits and the inhibition of the exaggerated sodium retention by ENaC inhibition. A similar pattern was observed under high salt (HS) diet conditions, where LS mice developed salt sensitivity. In an attempt to counteract sodium retention, the kidney achieves a neutral sodium balance through the pressure-natriuresis mechanism, where increased BP is associated with enhanced sodium excretion. However, when NMDA inhibitors are introduced in these animals, which already exhibit an activated pressure-natriuresis mechanism, continued decrease in BP can be observed. This effect is likely attributable to the inhibition of ENaC activity, further corroborating our proposed mechanism.

Notably, LS mice on HS diet displays evident sex differences in BP regulation. While male LS mice develop hypertension upon placement on HS diet, female LS mice do not exhibit the same salt sensitivity. Sex differences in BP regulation have been extensively documented across species, including humans[32]; however, prior reports on Liddle syndrome, either in human or animal studies, are relatively lacking. Generally, females exhibit greater protection against hypertension due to the protective effects of estrogen.[33] It has been demonstrated that estrogen negatively modulates sodium channels across the nephron, yet paradoxically, ENaC is not among these channels.[34,35] Instead, ENaC expression tends to be higher in females as we observed in the wildtype (Taconic) animals.[36] This finding indicate that female LS mice have a compensatory mechanism of increasing sodium excretion other than pressure-natriuresis, that can complement acute increase in sodium reabsorption. Given that risk of HTN increases substantially upon menopause and estradiol is known to have protective role on BP (16965722), the compensatory mechanism likely involves level of estrogen within female mice.[37] Correspondingly, we obtained data demonstrating that LS females have a better capacity to concentrate urine in comparison to males, reducing excessive water loss on a high salt diet (Appendix Figure 21), which will be the topic of future research.

To further investigate the NMDA receptor subtypes responsible for BP elevation and sex differences, we utilized the GluN2C-specific antagonist DQP997-74. This decision was based on previous reports indicating that GluN2C inhibits ENaC and that subunits *"2C"* and *"2D"* are the most frequently present in the connecting tubule. Our findings confirmed that GluN2C plays a central role in BP regulation, as the administration of a specific subunit inhibitor and the comparison of BP in genetic knockout (KO) mice models (grin2C and grin2D gene ablation) demonstrated that only GluN2C-KO mice exhibited elevated BP.

Gene transcription analysis comparing LS mice with WT mice did not reveal any genotype- or sex-specific differences. However, protein abundance analysis provided intriguing insights. WT mice on the 129/Sv background (Taconic) displayed the typical sex differences described for NMDA receptors, where females exhibit higher protein abundance. In contrast, LS mice

exhibited an inverse relationship, with male LS mice displaying nearly three times the protein levels compared to Taconic controls and higher levels than females. The discrepancy between RNAscope and IF quantification data suggests an intriguing conclusion in context of central dogma. At this point, we are unable to identify the specific post-transcriptional modifications that is regulating this difference in LS, but NMDA receptors and specifically GluN2C are subjected to phosphorylation (modulating trafficking), ubiquitination, glycosylation etc.[38]

Previous research has demonstrated that NMDA receptors exert a vasodilatory effect on the kidney.[39] The group of Thompson in California used microperfusion techniques to show that this vasodilatory effect originates from epithelial cells within the nephron and is independent of tubuloglomerular feedback.[40] Our group subsequently demonstrated that NMDA receptor activation stimulates CNTGF, while NMDA inhibition blunts CNTGF activation.[23] We hypothesized that NMDA inhibition with MK801 would decrease renal blood flow (RBF) due to CNTGF inhibition. However, acute experiments did not show significant net changes in RBF before and after MK801 infusion. This unexpected finding may be attributed to limitations in our segmented RBF evaluation using a small laser Doppler flow probe or compensatory mechanisms maintaining RBF homeostasis. Additionally, regional blood flow changes, particularly in the medullary circulation, may have occurred but were not captured due to our focus on cortical RBF.

Analyzing the RBF frequency by spectral analysis we evaluated possibles components altered in autoregulation.[15] Spectra analysis of RBF has shown several components[41,42]; there is a fast component on RBF oscillatory behavior located in the frequency range of 0.2-0.5 Hz which correspond to the tubular glomerular feedback (TGF), and a very slow frequency range mechanism, locate in the range of 0.008-0.01 Hz, which have been attributed to CNTGF mechanism. Spectral analysis of RBF revealed a decrease in the slow-frequency component (0.008 Hz) corresponding to CNTGF following MK801 administration, with no changes in the TGF component. Unexpectedly, an intermediate-frequency component (0.01–0.05 Hz) associated with neurogenic RBF regulation also decreased.[14] This suggests that NMDA inhibition may influence sympathetic activity, which is known to decrease RBF under conditions such as exercise and shock. Since MK801 is a CNS-active NMDA blocker, it is possible that the observed reduction in intermediate-frequency oscillations reflects a decrease in CNS-mediated sympathetic tone. This could, in turn, blunt the expected RBF reduction by counteracting CNTGF inhibition.

Previous scientific report has demonstrated that NMDA inhibition may induce change in blood pressure by releasing inhibitory effect in the NST, which indeed can have a transient increase in sympathetic activity.[43] Such change may correspond to reported psychotic and neurological side effects described for MK80.[45] Furthermore, ketamine—another known non-competitive NMDA inhibitor—infusion during depression treatment has reported side effect of HTN, which is presumably caused via the same mechanism as delineated above.[46] Of note, the interaction between CNS profile and blood pressure phenotype may be accentuated in LS

mice in particular; previous studies indicate that ENaC expressed in hypothalamus may drive the hypertensive phenotype, which would also display overactivation mutation of ENaC in case of LS mice.[47] While we cannot entirely rule out a CNS contribution to BP regulation following NMDA inhibition, our data demonstrate that a brain-impenetrant GluN2C inhibitor mimicked the same hypertensive response. Additionally, during acute intraperitoneal MK801 administration, no significant changes in BP or heart rate indicative of CNS effects were observed. However, prior studies indicate that MK801, also known as dizocilpine, induces rapid CNS tolerance within hours to days, potentially diminishing its central effects over time.[48] Future studies will explore the chronic impact of MK801 on renal hemodynamics to clarify these mechanisms.

Other mechanisms not constellated in these experiments may be in action. Thus, another plausible mechanism by which NMDA inhibition may contribute to acute elevation of blood pressure would be calcium-mediated endo/exocytosis of channels. In CNS, one of the calcium-mediated pathways by which synaptic clefts develop long term potentiation is by recruitment of additional synaptic AMPA receptors[49]; the pathway is regulated by intermediate signaling protein named synaptotagmin, which is responsible for vesicle exocytosis. Given that a class of synaptotagmin is expressed in the kidney[50] and disruption of proximal tubular endocytosis of salt transport may induce HTN, we can reasonably infer that renal NMDA receptors may regulate similar endo/exocytotic mechanism as that of synaptic cleft in CNS[51,52]; correspondingly, NMDA inhibition would induce acute BP elevation. Although the proposed mechanism displays weaker ties to the results discussed in this thesis, additional experiments validating relationship between presence of renal synaptotagmin and development of HTN could potentially endorse the actuality of this mechanism.

This thesis provides a more nuanced insight into how renal NMDA receptor affects RBF and blood pressure. The receptor's known relation to ENaC was exploited through utilization of LS mice, and cutting-edge biotechnology was used to evaluate the details of receptor expression in context of distinguishable levels of central dogma. We believe that clear understanding of renal NMDA receptor's involvement in various physiological processes can potentially establish a new branch of therapeutics that target medical conditions with renal etiology.

V. References

1. De Bhailis ÁM, Kalra PA. Hypertension and the kidneys. *Br J Hosp Med Lond Engl 2005*. 2022;83(5):1-11. doi:10.12968/hmed.2021.0440

2. Coffman TM. The inextricable role of the kidney in hypertension. *J Clin Invest*. 2014;124(6):2341-2347. doi:10.1172/JCI72274

3. Majid DSA, Prieto MC, Navar LG. Salt-Sensitive Hypertension: Perspectives on Intrarenal Mechanisms. *Curr Hypertens Rev*. 2015;11(1):38-48. doi:10.2174/1573402111666150530203858

4. Baek EJ, Kim S. Current Understanding of Pressure Natriuresis. *Electrolyte Blood Press E BP*. 2021;19(2):38-45. doi:10.5049/EBP.2021.19.2.3

5. Chmielewski C. Renal anatomy and overview of nephron function. *Nephrol Nurs J J Am Nephrol Nurses Assoc*. 2003;30(2):185-190; quiz 191-192.

6. Chmielewski C. Renal physiology series: Part 1 of 8. Renal anatomy and overview of nephron function. *ANNA J*. 1992;19(1):34-38.

7. Romero CA, Carretero OA. Tubule-vascular feedback in renal autoregulation. *Am J Physiol Renal Physiol*. 2019;316(6):F1218-F1226. doi:10.1152/ajprenal.00381.2018

8. McCormick JA, Ellison DH. Distal convoluted tubule. *Compr Physiol*. 2015;5(1):45-98. doi:10.1002/cphy.c140002

9. Wu P, Gao ZX, Zhang DD, et al. Effect of Angiotensin II on ENaC in the Distal Convoluted Tubule and in the Cortical Collecting Duct of Mineralocorticoid Receptor Deficient Mice. *J Am Heart Assoc*. 2020;9(7):e014996. doi:10.1161/JAHA.119.014996

10. Dalal R, Bruss ZS, Sehdev JS. Physiology, Renal Blood Flow and Filtration. In: *StatPearls*. StatPearls Publishing; 2025. Accessed March 10, 2025. http://www.ncbi.nlm.nih.gov/books/NBK482248/

11. Seikaly MG, Arant BS. Development of renal hemodynamics: glomerular filtration and renal blood flow. *Clin Perinatol*. 1992;19(1):1-13.

12. Wang H, Garvin JL, D'Ambrosio MA, Ren Y, Carretero OA. Connecting tubule glomerular feedback antagonizes tubuloglomerular feedback in vivo. *Am J Physiol Renal Physiol*. 2010;299(6):F1374-1378. doi:10.1152/ajprenal.00403.2010

13. Romero CA, Carretero OA. A Novel Mechanism of Renal Microcirculation Regulation: Connecting Tubule-Glomerular Feedback. *Curr Hypertens Rep*. 2019;21(1):8-8. doi:10.1007/s11906-019-0911-

14. Janssen BJ, Malpas SC, Burke SL, Head GA. Frequency-dependent modulation of renal blood flow by renal nerve activity in conscious rabbits. *Am J Physiol*. 1997;273(2 Pt 2):R597-608. doi:10.1152/ajpregu.1997.273.2.R597

15. Ryu H, Layton AT. Tubular fluid flow and distal NaCl delivery mediated by tubuloglomerular feedback in the rat kidney. *J Math Biol*. 2014;68(4):1023-1049. doi:10.1007/s00285-013-0667-5

16. Sgouralis I, Layton AT. Theoretical assessment of renal autoregulatory mechanisms. *Am J Physiol Renal Physiol*. 2014;306(11):F1357-1371. doi:10.1152/ajprenal.00649.2013

17. Jewett BE, Thapa B. Physiology, NMDA Receptor. In: *StatPearls*. StatPearls Publishing; 2025. Accessed March 10, 2025. http://www.ncbi.nlm.nih.gov/books/NBK519495/

18. Zhou C, Tajima N. Structural insights into NMDA receptor pharmacology. *Biochem Soc Trans*. 2023;51(4):1713-1731. doi:10.1042/BST20230122

19. Valdivielso JM, Eritja À, Caus M, Bozic M. Glutamate-Gated NMDA Receptors: Insights into the Function and Signaling in the Kidney. *Biomolecules*. 2020;10(7):1051. doi:10.3390/biom10071051

20. Du J, Li XH, Li YJ. Glutamate in peripheral organs: Biology and pharmacology. *Eur J Pharmacol*. 2016;784:42-48. doi:10.1016/j.ejphar.2016.05.009

21. Polychronopoulou E, Braconnier P, Burnier M. New Insights on the Role of Sodium in the Physiological Regulation of Blood Pressure and Development of Hypertension. *Front Cardiovasc Med*. 2019;6:136. doi:10.3389/fcvm.2019.00136

22. Navar LG, Von Thun AM, Zou L, el-Dahr SS, Mitchell KD. Enhancement of intrarenal angiotensin II levels in 2 kidney 1 clip and angiotensin II induced hypertension. *Blood Pressure Supplement*. 1995;2:88-92.

23. Romero CA, Lim J, Wang H, et al. Epithelial N-methyl-D-aspartate (NMDA) receptors mediate renal vasodilation by affecting kidney autoregulation. *BioRxiv Prepr Serv Biol*. Published online December 6, 2023:2023.12.04.569973. doi:10.1101/2023.12.04.569973

24. Enslow BT, Stockand JD, Berman JM. Liddle's syndrome mechanisms, diagnosis and management. *Integr Blood Press Control*. 2019;12:13-22. doi:10.2147/IBPC.S188869

25. Mubarik A, Anastasopoulou C, Aeddula NR. Liddle Syndrome (Pseudohyperaldosteronism). In: *StatPearls*. StatPearls Publishing; 2025. Accessed March 10, 2025. http://www.ncbi.nlm.nih.gov/books/NBK536911/

26. Pradervand S, Vandewalle A, Bens M, et al. Dysfunction of the epithelial sodium channel expressed in the kidney of a mouse model for Liddle syndrome. *J Am Soc Nephrol JASN*. 2003;14(9):2219-2228. doi:10.1097/01.asn.0000080204.65527.e6

27. Mutchler SM, Kirabo A, Kleyman TR. Epithelial Sodium Channel and Salt-Sensitive Hypertension. *Hypertens Dallas Tex 1979*. 2021;77(3):759-767. doi:10.1161/HYPERTENSIONAHA.120.14481

28. Wang H, Su N, Wang LC, et al. Quantitative ultrasensitive bright-field RNA in situ hybridization with RNAscope. *Methods Mol Biol Clifton NJ*. 2014;1211:201-212. doi:10.1007/978-1-4939-1459-3_16

29. Sari AIP, Copeland K, Nuwongsri P, et al. RNAscope Multiplex FISH Signal Assessment in FFPE and Fresh Frozen Tissues: The Effect of Archival Duration on RNA Expression. *J Histochem Cytochem Off J Histochem Soc*. 2025;73(1-2):9-28. doi:10.1369/00221554241311971

30. Ren Y, Janic B, Kutskill K, Peterson EL, Carretero OA. Mechanisms of connecting tubule glomerular feedback enhancement by aldosterone. *Am J Physiol Renal Physiol*. 2016;311(6):F1182-F1188. doi:10.1152/ajprenal.00076.2016

31. Shemin D, Dworkin LD. Sodium balance in renal failure. *Curr Opin Nephrol Hypertens*. 1997;6(2):128-132. doi:10.1097/00041552-199703000-00004

32. Reckelhoff JF. Gender differences in hypertension. *Curr Opin Nephrol Hypertens*. 2018;27(3):176-181. doi:10.1097/mnh.0000000000000404

33. Reckelhoff JF. Mechanisms of sex and gender differences in hypertension. *J Hum Hypertens*. 2023;37(8):596-601. doi:10.1038/s41371-023-00810-4

34. Veiras LC, Girardi ACC, Curry J, et al. Sexual Dimorphic Pattern of Renal Transporters and Electrolyte Homeostasis. *J Am Soc Nephrol JASN*. 2017;28(12):3504-3517. doi:10.1681/ASN.2017030295

35. Li Q, McDonough AA, Layton HE, Layton AT. Functional implications of sexual dimorphism of transporter patterns along the rat proximal tubule: modeling and analysis. *Am J Physiol Renal Physiol*. 2018;315(3):F692-F700. doi:10.1152/ajprenal.00171.2018

36. Hu R, McDonough AA, Layton AT. Functional implications of the sex differences in transporter abundance along the rat nephron: modeling and analysis. *Am J Physiol Renal Physiol*. 2019;317(6):F1462-F1474. doi:10.1152/ajprenal.00352.2019

37. Ashraf MS, Vongpatanasin W. Estrogen and hypertension. *Curr Hypertens Rep*. 2006;8(5):368-376. doi:10.1007/s11906-006-0080-1

38. Tahiri E, Corti E, Duarte CB. Regulation of Synaptic NMDA Receptor Activity by Post-Translational Modifications. *Neurochem Res*. 2025;50(2):110. doi:10.1007/s11064-025-04346-6

39. Deng A, Valdivielso JM, Munger KA, Blantz RC, Thomson SC. Vasodilatory N-Methyl-D-Aspartate Receptors Are Constitutively Expressed in Rat Kidney. *J Am Soc Nephrol*. 2002;13(5):1381-1384. doi:10.1097/01.asn.0000013293.11876.4e

40. Deng A, Thomson SC. Renal NMDA receptors independently stimulate proximal reabsorption and glomerular filtration. *Am J Physiol Renal Physiol*. 2009;296(5):F976-982. doi:10.1152/ajprenal.90391.2008

41. Sgouralis I, Maroulas V, Layton AT. Transfer Function Analysis of Dynamic Blood Flow Control in the Rat Kidney. *Bull Math Biol*. 2016;78(5):923-960. doi:10.1007/s11538-016-0168-y

42. Ryu H, Layton AT. Tubular fluid flow and distal NaCl delivery mediated by tubuloglomerular feedback in the rat kidney. *J Math Biol*. 2014;68(4):1023-1049. doi:10.1007/s00285-013-0667-5

43. Lewis SJ, Barres C, Jacob HJ, Ohta H, Brody MJ. Cardiovascular effects of the N-methyl-D-aspartate receptor antagonist MK-801 in conscious rats. *Hypertens Dallas Tex 1979*. 1989;13(6 Pt 2):759-765. doi:10.1161/01.hyp.13.6.759

44. Tian B, Hartle DK. Cardiovascular effects of NMDA and MK-801 infusion at area postrema and mNTS in rat. *Pharmacol Biochem Behav*. 1994;49(3):489-495. doi:10.1016/0091-3057(94)90060-4

45. Janus A, Lustyk K, Pytka K. MK-801 and cognitive functions: Investigating the behavioral effects of a non-competitive NMDA receptor antagonist. *Psychopharmacology (Berl)*. 2023;240(12):2435-2457. doi:10.1007/s00213-023-06454-z

46. Ansari M, Pittman B, Tylee DS, Ostroff R, Wilkinson ST, Nikayin S. Blood pressure changes during ketamine infusion for the treatment of depression. *Gen Hosp Psychiatry*. 2024;90:62-67. doi:10.1016/j.genhosppsych.2024.07.001

47. Mills NJ, Sharma K, Haque M, Moore M, Teruyama R. Aldosterone Mediated Regulation of Epithelial Sodium Channel (ENaC) Subunits in the Rat Hypothalamus. *Neuroscience*. 2018;90:278-292. doi:10.1016/j.neuroscience.2018.08.031

48. Wessinger WD. Tolerance to and dependence on MK-801 (dizocilpine) in rats. *Pharmacol Biochem Behav*. 1994;49(4):1049-1056. doi:10.1016/0091-3057(94)90263-1

49. Wu D, Bacaj T, Morishita W, et al. Postsynaptic synaptotagmins mediate AMPA receptor exocytosis during LTP. *Nature*. 2017;544(7650):316-321. doi:10.1038/nature21720

50. Kishore BK, Wade JB, Schorr K, Inoue T, Mandon B, Knepper MA. Expression of synaptotagmin VIII in rat kidney. *Am J Physiol*. 1998;275(1):F131-142. doi:10.1152/ajprenal.1998.275.1.F131

51. Chen M, Gu X. Emerging roles of proximal tubular endocytosis in renal fibrosis. *Front Cell Dev Biol*. 2023;11:1235716. doi:10.3389/fcell.2023.1235716

52. Wang X, Armando I, Upadhyay K, Pascua A, Jose PA. The regulation of proximal tubular salt transport in hypertension: an update. *Curr Opin Nephrol Hypertens*. 2009;18(5):412-420. doi:10.1097/MNH.0b013e32832f5775

VI. Appendix

a. RNAscope Technique Validation Supplementary Data

We validated the RNAscope technique on brain and kidney tissues from C57b6 wildtype animals (Figure 20). "Negative Control" probe (provided in RNAscope assay kit) was utilized for generation of valid negative control imaging.

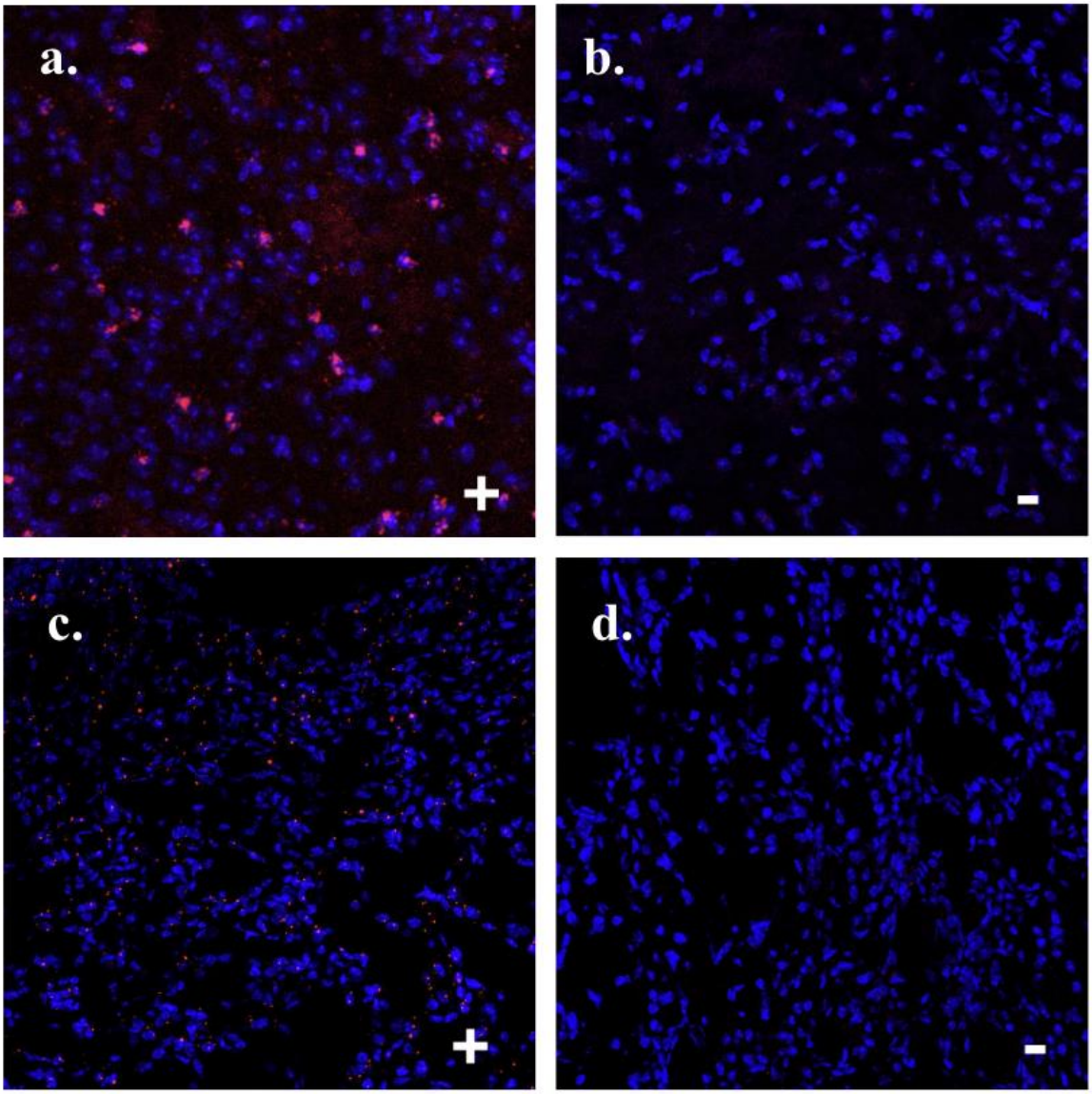

Figure 20: RNAscope technique validation. (a.) Grin2C detection with RNAscope assay in C57 WT mice brain tissue versus (b.) negative control. (c.) Grin2C detection with RNAscope assay in C57 WT mice kidney tissue versus (d.) negative control.

b. NeuroMab Antibody Supplementary File

GluN2C antibody (hosted in mice) utilized in IF experiment was validated in Emory School of Medicine Department of Pharmacology and published by NeuroMab:

https://neuromab.ucdavis.edu/datasheet/N422_18.pdf

c. Urine Collection and Osmolarity Analysis Supplementary Data

Excretion level of sodium and potassium ion via urine can provide critical insight on the longitudinal effect of NMDA inhibition. Correspondingly, Na^+/K^+ ratio in urine was evaluated alongside blood pressure. Mice were individually placed into an empty cage without bedding, and spot urine was collected via micropipette. Subsequently, ion concentration of the urine was measured via EasyLyte electrolyte analyzer; the probe of the machine was inserted to an Eppendorf with diluted volume of urine samples, and the results were recorded accordingly.

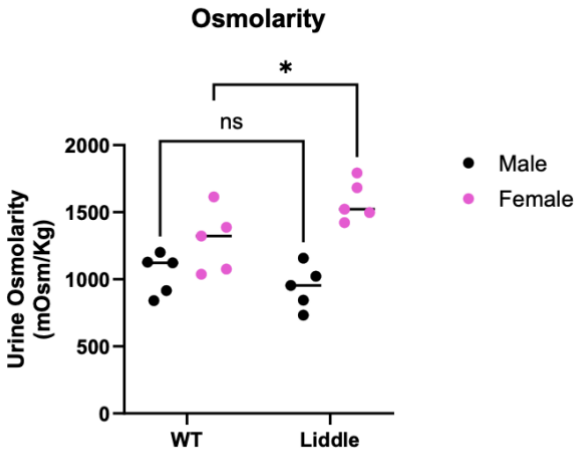

Figure 21: Urine Osmolarity of WT versus LS mice. Female LS cohort exhibits elevated urine osmolarity compared to the WT counterpart that is statistically significant, while LS male cohort does not.